PHILIPS

Application book

Electronic components and materials

D.C. Motors with Ferroxdure permanent magnets

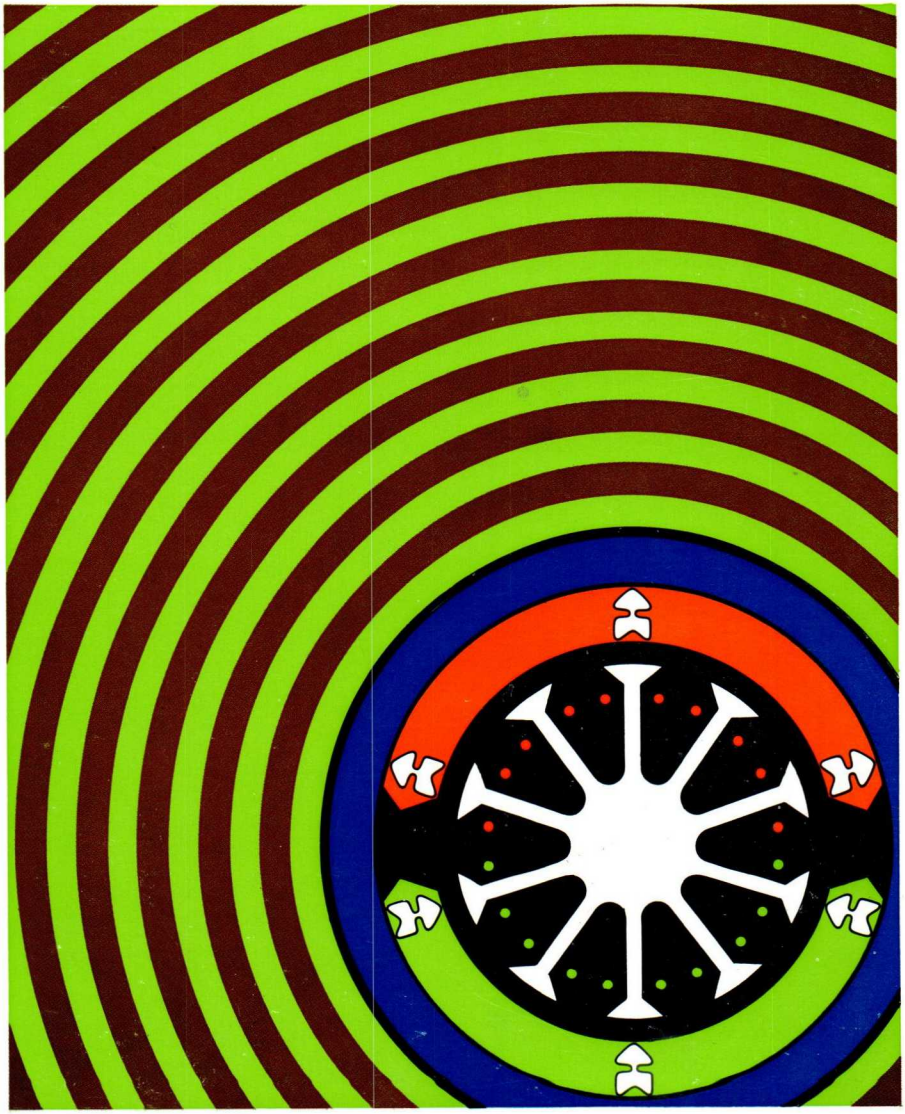

D.C. Motors with Ferroxdure Permanent Magnets

D.C. Motors with Ferroxdure Permanent Magnets

PUBLICATIONS DEPARTMENT
ELECTRONIC COMPONENTS AND MATERIALS DIVISION

© *N.V. Philips' Gloeilampenfabrieken, Eindhoven, The Netherlands*

September 1974

The publication of this document does not imply a licence under any patent

Contents

Introduction 1

1 **General Concepts of Magnetism** 3
1.1 Magnetic Field Strength 3
1.2 Magnetic Flux and Induction 3
1.3 Magnetic Polarization 5
1.4 Hysteresis Loop 5
1.5 Initial Permeability, Recoil Permeability 7
1.6 Demagnetization, Demagnetizing Curve 7
1.7 Magnetic Potential, Magnetic Conductivity 8

2 **Magnetic Circuit Analysis** 9
2.1 Fundamental Equations 9
2.2 Magnet Volume and Optimum Working Point 10
2.3 Dimensions of the Magnet 12
2.4 Example of Calculation 12
2.5 The Load Line 13
2.6 Energy in the Magnetic Circuit 14
2.7 Shift of the Working Point by External Fields and Changes in the Air Gap 15
2.8 Temperature Changes in a Magnetic Circuit 20

3 **D.C. Motors with Permanent Magnets** 25
3.1 General 25
3.2 Magnets in Motors 26
3.3 Stator Housing 30
3.4 Designing a Permanent Magnet Motor 30
3.5 Multipole Motor Design 40

4 **Dimensions and Tolerances of Magnets for D.C. Motors** 42

5 **Magnetisation and Demagnetization** 45
5.1 Equipment for Generating Magnetization Currents 45
5.1.1. D.C.-magnetization Equipment 46
5.1.2 Half-cycle Magnetizers 46
5.1.3 Capacitor Discharge Magnetizers 48
5.1.4 Pulse Transformers 52
5.2 Coils for Magnetizing Rings and Segments for D.C. Motors 54
5.3 Magnetizing Yoke 56
5.4 Flux Measurement and Stabilization 59
Appendix 64

Acknowledgement

This book has been compiled by J. H. v.d. Valk, late of Philips Product Division Electronic Components and Materials, and is based upon material contained in 'Magnadure magnets for d.c. Motors', published by Mullard Limited, U.K., and 'Permanentmagnete', published by Valvo G.m.b.H, Germany. Additional material was supplied by W. A. Ledeboer, Philips ELCOMA.

Introduction

Growing world prosperity has brought about an ever increasing demand for battery operated electric motors. Not only cars, but also an abundance of home appliances, tools and out-door equipment make use of d.c. motors. Examples are windscreen wipers and other auxiliary motors in cars, battery shavers, carving knives, toys etc. The design of such motors should represent the best compromise between engineering and economic requirements.

The constant magnetic field required for a d.c. motor can be provided either by a direct current flowing through field windings or by permanent magnets. The latter has considerable advantages because for a given power the volume of a permanent magnet motor can be less than that of the equivalent wound-field type. The weight is lower, and the elimination of the field coils reduces the risk of insulation failures, thus reducing maintenance cost and increasing reliability. The armature reaction of a permanent magnet motor and its heat development are also lower.

The magnets can be of the metal alloy type or of the ceramic type. In motor applications ferroxdure magnets offer various advantages over metal alloy magnets. Without elaborating on this subject we mention: shorter magnets, resulting in smaller motor diameter – no pole shoes required – stable against demagnetizing magnetic fields – generally less costly since ferroxdure does not contain expensive metals much as cobalt or nickel.

This book deals exclusively with ferroxdure magnets.

Note on units

In recent years, considerable progress has been made towards the adoption of a single system of units by both science and industry. In 1960 an internationally agreed system of units was introduced, the "Système International d'Unités"; SI units are used in this book.

However, since some of the fundamental SI units (metre for length, kilogramme for mass, and ampere for current) result in magnetic units that are sometimes large for practical work with permanent magnets, the older c.g.s. system is still used widely in this field. A table for converting SI units to c.g.s. and vice versa is given below. The table also gives some practical decimal sub-multiples of SI units.

Conversion Table Magnetic Units

1 gauss (Gs)	$= 10^{-4}$ tesla $= 0{,}1$ millitesla
1 oersted (Oe)	$= 79{,}6$ A/m $= 0{,}796$ A/cm or T.A/m (cm).
1 maxwell (Mx)	$= 10^{-8}$ weber $= 10^{-2}$ μWb
1 gauss oersted (G.Os)	$= 7{,}96 \times 10^{-3}$ J/m^3 $= 7{,}69 \times 10^{-6}$ mJ/cm^3 $=$ $\pi/4$ T.A/m
1 tesla (T)	$= 1$ V.s/m^2 $= 10^{-4}$ V.s/cm^2 $= 10^4$ gauss
1 mT	$= 10$ gauss
1 A/m	$= 1{,}257 \times 10^{-2}$ oersted
1 A/cm	$= 100$ A/m $= 1{,}257$ oersted
1 weber (Wb)	$= 1$ V.s. $= 1$ Tm^2 $= 10^8$ maxwell
1 μWb	$= 100$ maxwell
1 joule/m^3	$=$ T.A/m $= 125{,}7$ gauss-oersted
1 mJ/cm^3	$= 1$ kJ/m^3 $= 125{,}7 \times 10^3$ gauss-oersted
μ_o	$= 4\pi \times 10^{-7} = 1{,}257 \times 10^{-6}$ (V.s/A.m $=$ H/m)
1 newton (N)	$= 1$ V.A.s

1 General Concepts of Magnetism

In this section the laws of magnetism, magnetic units and their main relationships will be treated. The theme will be the derivation of the equations necessary for magnetic calculations.

1.1 Magnetic Field Strength

Let a direct current of I amperes flow through a closely wound long solenoid of N turns and having a total length of l metres. The field strength in the middle of the coil is now defined as

$$H = \frac{NI}{l} \quad (\mathrm{A/m}). \tag{1}$$

This means that in such a coil the field strength can be determined by a simple measurement of the current. Such field can be used for calibrating a magnetometer, consisting of a short pivoted compass needle the torque of which, affected by the field, is measured.

Instead of the A/m which is the SI unit of field strength often the old c.g.s. unit "oersted" is used, suitable corrections being applied.

1.2 Magnetic Flux and Induction

The field strength of 1.1 gives rise to a magnetic induction B. *In vacuo* this induction is proportional to the field strength:

$$B = \mu_o H \quad \left(\frac{\mathrm{V \cdot s}}{\mathrm{m^2}} = \mathrm{tesla}\right). \tag{2}$$

The factor μ_o is called the permeability of vacuum. It is equal to:

$$\mu_o = 1{\cdot}257 \times 10^{-6} \quad \left(\frac{\mathrm{V \cdot s}}{\mathrm{A \cdot m}}\right). \tag{3}$$

If instead of being evacuated, the space within the solenoid is filled with some non-magnetic medium, the proportionality between B and H is maintained.

However, a different factor has to be used, depending on the medium in question.

We then have

$$B = \mu H = \mu_r \mu_o H. \tag{2a}$$

μ is the absolute permeability, and $\mu_r = \mu/\mu_o$ is the relative permeability. For non-ferromagnetic materials μ_r may be taken as unity for most practical purposes.

Ferromagnetic and ferrimagnetic materials however, possess a virtually higher relative permeability; the numerical value of μ_r moreover changes with the field strength H and also depends on the previous treatment of the material (see Hysteresis, Loop Section 1.4).

The induction, i.e. the specific magnetic flux in a magnetic field, can be determined by extracting a small search coil from the field and measuring the voltage generated between the terminals of the probe.

Faraday's law gives:

$$\int E = N \frac{\mathrm{d}\phi}{\mathrm{d}t} \quad (\mathrm{V}), \tag{4}$$

where N = number of turns of the search coil.

The voltage should be measured with an instrument, e.g. a ballistic galvanometer, of which the oscillating time is large compared with the time in which the coil is extracted from the field. We then measure the integral of Faraday's law:

$$E \cdot \mathrm{d}t = N\phi$$

which yields $\phi = Et/N$.

This divided by the area A of the search coil gives

$$B = \frac{E\,t}{N\,A} \quad (\mathrm{V.s/m^2}) = \text{tesla}). \tag{5}$$

If the area A is not normal to the direction of the flux, but forms an angle ϕ with this direction, then

$$B = \frac{E\,t}{N\,A \cos\phi}. \tag{5a}$$

The relation between SI and c.g.s. systems is: 1 tesla $= 10^4$ gauss. A fluxmeter is the instrument normally used for practical measurements.

1.3 Magnetic Polarization

Two kinds of fields determine the induction B of a magnetic material in a magnetic field. The first is the field H, originating from a coil, some exterior field or, in the case of an open magnetic circuit, from its own demagnetizing field.

The second field is the one evoked by the elementary magnets in the matter; this last field is called the magnetization M. So

$$B = \mu_o H + \mu_o M. \tag{6}$$

The value $\mu_o M$ is called the magnetic polarization J. In other words

$$B = \mu_o H + J. \tag{7}$$

The induction accordingly is built up from two parts, the first one $\mu_o H$ is always present, even *in vacuo*, if a field H exists; the second one represents the additional induction generated by the elementary magnets forming the material of which the magnetic circuit is made.

From eqs (6) and (7) it will be clear that J can be expressed in V.s/m^2 or tesla, whereas M has the dimension A/m.

1.4 Hysteresis Loop

When the polarization J or the induction B of a ferromagnetic body that is being subjected to a magnetic field for the first time, is plotted against this field, an initial curve is obtained starting at the origin (Fig. 1).

With increasing field strength H this curve approaches a straight line. In the case of J being plotted this line runs parallel to the H-axis; if B is plotted it has a slope parallel to the line $\mu_o H$.

The material is now magnetically saturated; the saturation polarization has been reached and a further increase of the field would not further increase the polarization.

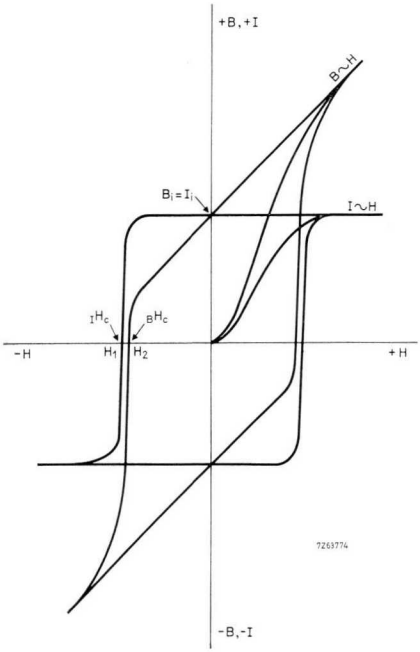

Fig. 1 $B = f(H)$ and $J = f(H)$ loops of anisotropic Ferroxdure.

When the field is now decreased, a curve is described that is basically different from the initial curve. Induction and polarization do not entirely disappear when the field is reduced to zero. In the case of a closed ring of uniform cross-section the remaining induction, which is equal to the polarization ($B_r = J_r$), is called remanence. To reduce B and J to zero, reverse fields are required, that are respectively called coercive field strength ($_BH_c$) and intrinsic coercive field strength ($_IH_c$). The values of these two fields differ. For Ferroxdure the differences may be from 500 to 50 000 A/m.

A further increase of the reverse field leads to saturation again, this time in the third quadrant of the graph. From there, reduction of the field produces the lower part of the hysteresis loop until saturation is reached again. Fig. 1 shows both the $B(H)$ and the $J(H)$ loops.

With a ring of ferromagnetic material the form of the hysteresis loop only depends on the material used. All ceramic permanent magnet materials have coercive field strengths well over 10^5 A/m.

1.5 Initial Permeability, Recoil Permeability

The slope of the initial curve near to the origin is called the initial permeability of the material. It is expressed as the tangent of the angle formed by the curve and the abscissa. The permeability at an arbitrary point of the loop is defined by the slope of the tangent at this point.

The recoil permeability is the gradient in the second quadrant along which the working point (q.v.) is moving as a consequence of small alterations in the demagnetizing field.

1.6 Demagnetization, Demagnetizing Curve

Magnetic data and hysteresis loops published in catalogues and technical papers always refer to closed magnetic circuits (e.g. rings) of ferromagnetic material. When no external field is present such a circuit will, after saturation, remain in the remanent state ($B_r = J_r$) since there is no self demagnetizing field present since the field lines cannot leave the material.

When an air gap is present there is a demagnetizing field H_{de} caused by the free poles. If the gap is small compared to the circular length of the ring, or if we have a long rod of permanent magnet material, with good approximation

$$H_{de} = -N_{de} M, \tag{8}$$

where M is the magnetization, and N_{de} the demagnetizing factor having a value between 0 and 1 depending on the shape of the circuit.

From eqs (6), (7) and (8) it follows:

$$J = -\frac{\mu_o H_{de}}{N_{de}} \tag{9}$$

or

$$B = -\mu_o \frac{1 - N_{de}}{N_{de}} H_{de}. \tag{10}$$

Eqs (9) and (10) represent the load line of the magnet in the $J(H)$ and $B(H)$ diagrams (see Section 2, "Magnetic Circuit Analysis").

The load line cuts the hysteresis loop at two points, namely in the second and fourth quadrants. We generally consider J or B as positive so only the

second quadrant is used in practice. This part of the hysteresis loop is called the demagnetization curve.

The main properties of a permanent magnet material are characterized by three points on the demagnetization curve:

1. the *remanence* B_r $(H = 0)$;
2. the *coercive force* ${}_BH_c$ $(B = 0)$ or ${}_JH_c$ $(J = 0)$.
3. the $(BH)_{max}$ *point*, i.e. the point B_d, H_d chosen in such a way that the product $B_d \times H_d$ is maximum.

This product is a measure for the quality of the material. In many cases it denotes the optimum working point on the BH curve.

1.7 Magnetic Potential, Magnetic Conductivity

Magnetic calculations are often simplified by the introduction of the concept of magnetic potential and magnetic conductivity. This may result in analogies between magnetic and electric circuits. The magnetic potential is defined as the line integral of the magnetic field strength between the points A and B of a flux path s. The points A and B have magnetic potential V_A and V_B so that

$$V_B - V_A = V_{BA} = \int_A^B H ds. \tag{11}$$

In a magnetic circuit with an air gap the maximum potential difference is normally between two opposite planes on either side of the gap.

We then define the conductivity as

$$\Lambda = \frac{\phi}{V} \tag{12}$$

where ϕ is the magnetic flux between the two planes.

The reciprocal

$$R = \frac{V}{\phi} \tag{13}$$

is called the magnetic resistance or reluctance.

2 Magnetic Circuit Analysis

This section deals with the calculation of magnet dimensions. Special attention is given to the influence of stray fields.

2.1 Fundamental Equations

The starting point is Maxwell's law that in a magnetic circuit the line integral of field strength is zero.

$$\oint H dl = 0.$$

That is that the magneto-motive force (m.m.f.) the air gap is equal but opposite to that in the magnet

$$H_M L_M = -H_g L_g \tag{14}$$

where H_M and H_g are the field strengths in the magnet and in the air gap and L_M and L_g the respective lengths.

In practice a factor q is added, to compensate for m.m.f. loss caused by extra reluctance from the soft iron pole shoes, and their transient planes:

$$H_M L_M = -q H_g L_g. \tag{15}$$

This factor q has a value of 1,05 to 1,25. If the soft iron is still far from saturation, the low value is generally adequate.

The total flux ϕ_{tot} in a static magnetic circuit is always constant. It can be divided into two parts, the useful flux in the air gap, ϕ_g, and the stray flux ϕ_s.

The stray factor is defined as

$$p = \frac{\phi_{tot}}{\phi_g}.$$

So

$$\phi_{tot} = p\phi_g = pB_g A_g = B_M A_M \tag{16}$$

where A_g and A_M are the cross-sections of air gap and magnet. B_g is the induction in the gap; B_M is the mean induction in the neutral plane of the magnet.

The stray factor is a decisive factor for calculating magnetic circuits. Practical values lie between 1,2 and 10, depending on the geometric design and the dimensions of magnet, pole pieces and air gap.

The connection between the field strength or induction in the magnet and that in the air gap is given by eqs (15) and (16).

For our calculation we furthermore need to know the relationship between field strength and induction both in the air gap and in the magnet.

In the air gap the induction is always proportional to the field as stated in eq. (2)

$$B_g = \mu_o H_g.$$

The relationship between B and H in the magnet is given by the demagnetization curve of the permanent magnet material to be used:

$$B_M = f(H_M). \tag{17}$$

For most permanent magnet materials this curve is published by the manufacturers.

With the aid of these data a magnetic circuit can be designed. In the first instance the values for q and p should be estimated.

2.2 Magnet Volume and Optimum Working Point

It is clear from eqs (15) and (16) that a high value of H of the magnetic material results in a short magnet and that a high value of B gives a small magnet cross-section. Ferroxdure, having a high coercive force and a comparatively low remanence, will in general lead to short magnets of a large cross-section.

Multiplication of eqs (15) and (16) yields

$$q\,p\,\frac{B_g^{\,2}}{\mu_o} A_g L_g = B_M H_M A_M L_M, \tag{18}$$

from which it can be seen that for a given induction in an air gap of given dimensions the magnet volume $A_M L_M$ is in inverse proportion to the product $B_M H_M$. It is therefore appropriate to work in that part of the BH curve where the product (BH) is maximum. This applies to so-called static applications where the working point is not shifted during operation or by significant temperature fluctuations.

The $(BH)_{max}$ values are indicated in the material tables. Those for Ferroxdure can be found in the Appendix. When a set of hyperbolae for $(BH) =$ constant is drawn in the second quadrant the demagnetization curve just touches the one for $BH = (BH)_{max} =$ constant.

The coordinates of this point give the B_d and H_d values corresponding to this $(BH)_{max}$.

A good approximate method for obtaining the $(BH)_{max}$ point is to draw a rectangle with B_r and H_c as sides. The diagonal of this rectangle intersects the BH curve at a point that for practical purposes may be considered as the $(BH)_{max}$ point (see Fig. 2).

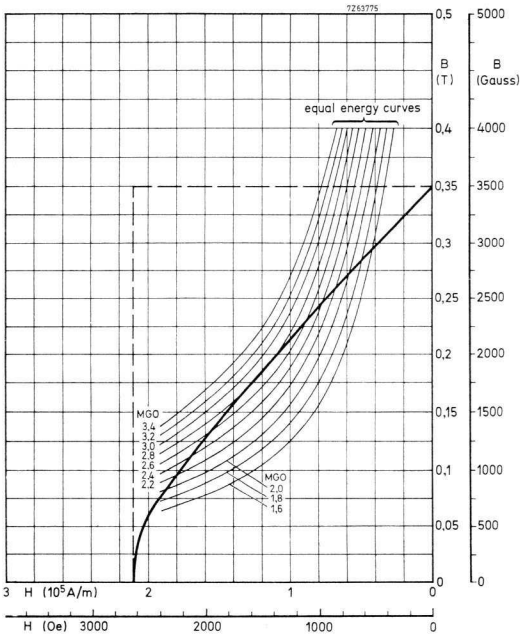

Fig. 2 Demagnetization curve showing $(BH)_{max}$.

2.3 Dimensions of the Magnet

If the air gap requirements are known and the stray factors q and p have been estimated, eqs (15), (16) and (17) still contain four unknowns, B_M, H_M, A_M and L_M. This means that we are free to fix one. With a view to the foregoing section $H_M = H_d$ is generally chosen as we prefer the system to be working in the $(BH)_{max}$ point. From the demagnetization curve of the preferred magnet material we can then also read B_d. From eqs (15) and (16) we can derive

$$L_M = \frac{q\, B_g\, L_g}{\mu_o\, H_M} \tag{19}$$

and

$$A_M = \frac{p\, B_g\, A_g}{R_L}. \tag{20}$$

It goes without saying that, apart from magnetic, mechanical considerations also affect the ultimate design of a circuit. This will be particularly so if Ferroxdure is used, since requirements of mechanical strength must be met.

2.4 Example of Calculation

Let a magnet be required that in a static system gives an induction of 900 mT (9000 gauss) in air gap of 3 mm length and 2 cm² cross-section. If the factors q and p are estimated at 1,05 and 3 respectively and if Ferroxdure 300 is used, the following data can be substituted in eqs (19) and (20):

$L_g = 3 \times 10^{-3}$ m;
$A_g = 2 \times 10^{-4}$ m²;
$B_g = 0{,}9$ T;
$H_d = 14 \times 10^4$ A/m
$B_d = 0{,}2$ T } taken from material data available;
$q = 1{,}05$;
$p = 3$;
$\mu_o = 1{,}256 \times 10^{-6}$.

This yields:

$L_M = 1{,}6$ cm,
$A_M = 27$ cm².

With a magnet disc of 58,5 cmm diameter and a thickness of 16 mm the requirements can apparently be met, with the magnet working near the $(BH)_{max}$ point.

The only way to check whether the assumption $p = 3$ was correct, is to have a magnet system made with a magnet of the dimensions just found and to measure the actual flux in the air gap.

When this is lower than the requirements, the p value might have been taken too low and a higher value will have to be substituted in eq. (20). Also saturation might occur in the soft iron pole pieces. This could be remedied by increasing their cross-sections. The errors may be assessed by measurements made on the model.

2.5 The Load Line

When dividing eq. (16) by eq. (15) we find

$$\frac{B_M}{\mu_o H_M} = \frac{p\, B_g\, A_g\, L_M}{q\, \mu_o\, H_g L_g\, A_M} = \mu_o \frac{p}{q} \times \frac{A_g}{L_g} \times \frac{L_M}{A_M}. \tag{21}$$

In other words, the ratio between induction and field strength in a magnet depends only on the dimensions of magnet and air gap (apart from q and p), that is, on the geometry of the magnetic circuit. It is independent of the quality of the magnet material or the induction in the air gap.

In the demagnetization curve (Fig. 3) the ratio B/H is indicated by a straight line that forms an angle α with the B-axis, so that cotan $\alpha = B/H$. This load line is defined by the geometry of the magnetic circuit. It intersects the demagnetization curve at the working point P.

The aim is to design * the circuits so as to have P coinciding with the $(BH)_{max}$ point of the BH curve. When this is the case for a specific magnet material, it will almost certainly not be so for a different material. In Fig. 3 a second demagnetization curve has been drawn, intersecting the load line in P'.

Though material 2 may have a higher $(BH)_{max}$ value, this has no advantage in this particular case, since the actual product $B_M{}'H_M{}'$ is smaller than $B_M H_M$.

This means that for each magnet material the circuit has to be redesigned in order to take full advantage of the material properties.

* For simple static applications.

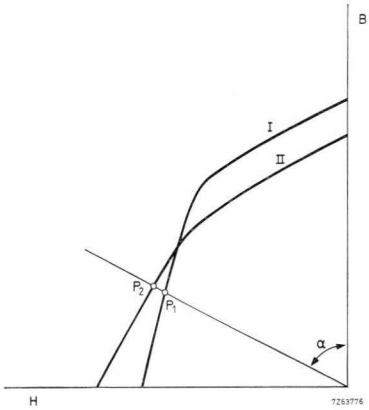

Fig. 3 Load line of a magnetic circuit. Though material *I* has a higher $(BH)_{max}$ value than material *II*, the induction *B* at the working point is lower for material *I*.

2.6 Energy in the Magnetic Circuit

Assume a circuit with an air gap in which all stray flux is represented by a second air gap, Fig. 4. The total flux through the magnet is then divided in two parts. The working flux ϕ_g and the stray flux ϕ_s.

We then may write

$$\phi_M = \phi_g + \phi_s \tag{22}$$

or

$$B_M A_M = B_g A_g + B_s A_s. \tag{23}$$

When there is no reluctance in the mild steel, ($q = 1{,}0$), the field strength in the magnet is equal to the field strengths in both air gaps:

$$-H_M L_M = H_g L_g + H_s L_s. \tag{24}$$

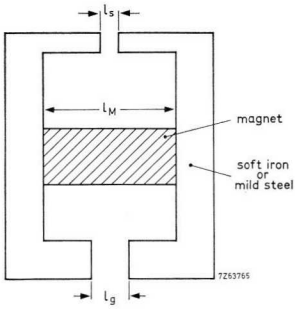

Fig. 4 Permanent magnet with useful air gap L_g, and stray gap L_s.

Multiplication of eqs (23) and (24) yields

$$-B_M H_M V_M = B_g H_g V_g + B_s H_s V_s. \tag{25}$$

The left hand term represents the (double) energy of the magnet **, the right-hand term is the (double) sum of the useful energy and the stray energy. The sum of all energies is zero, which means that no energy leaves the system. This is valid irrespective of the working point of the magnet.

2.7 Shift of the Working Point by External Fields and Changes in the Air Gap

STABILIZATION

External magnetic fields or changes in air gap width will shift the position of the working point on the BH-curve.

The former causes a parallel displacement of the load line, whereas the latter causes a change in the angle α, formed with the B-axis.

** A negative value should always be assigned to the field strength H_M. The minus sign in eq. (24) results in a positive energy.

The external field, H_{ext}, superposed in an open magnetic circuit, i.e. a circuit with air gap, differs from the internal field H by an amount equal to the demagnetizing field $H_{de} = -N_{de}M$ (see eq. (8)).

So

$$H_{ex} = H + N_{de}M. \tag{26}$$

Since from eq. (6) it follows that

$$M = \frac{B}{\mu_o} - H \tag{27}$$

elimination of M in eq. (26) yields

$$B = \frac{\mu_o}{N_{de}} H_{ext} - \mu_o \frac{1 - N_{de}}{N_{de}} H. \tag{28}$$

This means that the external field H_{ex} causes a parallel shift of the load line. For $H_{ext} = 0$ eq. (28) is identical to eq. (10). As we are working in the second quadrant the value of H is always negative. If H_{ex} is in the same direction (also negative) the result will be a reduction of the induction B and consequently of the field strength in the air gap.

The distance over which the load line will shift along the H-axis can be calculated from eq. (28) by putting $B = 0$:

$$H_B = 0 = \frac{H_{ex}}{1 - N_{de}}. \tag{29}$$

This shows that the shifting will be greater for high values of N_{de} and thus largely depends on the geometrical shape of the magnet (and the circuit).

The new working point is the point of intersection of the demagnetizing curve and the parallel shifted load line. This is true only if the external field weakens the induction. When it tends to enlarge the field strength in the air gap, the new working point is found in this way only if the working area is in the straight, flat part of the demagnetization curve. Otherwise a lower working point will be obtained.

In Fig. 5 the working point P_1 is shifted to P_2 by the influence of an external field.

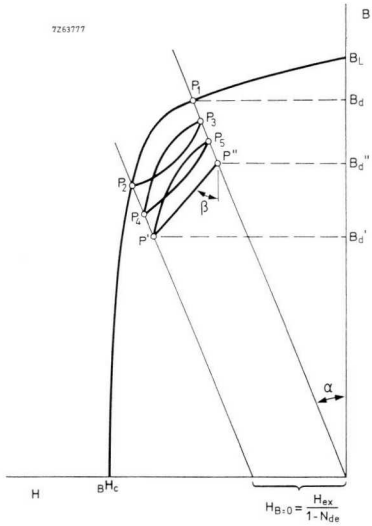

Fig. 5 Shift of load line by an external field. Repeated switching on and off of this field results in stabilization of the working point.

When this field is removed the working point does not follow the demagnetization curve back to P_1, but arrives at a point P_3 on the load line, somewhat below P_1. When the field is applied and removed again, P_4 and P_5 are the respective new working points.

After a few repetitions of this procedure, stabilization is reached. The working point now moves along a line $P'P''$. Only an increased external field would give lower working points. The slope of the line $P'P''$ runs parallel to the upper part of the demagnetization curve. With Ferroxdure the cotangent of the angle, formed with B-axis, the recoil permeability μ_{rev}, is approx. 1,05.

The same reasoning holds if the shifting of the working point is not caused by an external field, but by a change in the air gap length. In that case we do not have a parallel displacement of the load line, but a variation of the angle α formed between load line and B-axis. The results is the same: stabilization is

achieved, the working point varies between P' and P'', and the induction between B_M' and B_M'', see Fig. 6. From Figs 5 and 6 it can be seen that the points P_1 and P_2 are on either side of the knee in the demagnetization curve. This causes the ultimate differences B_M and B_M'. When, however, P_1 and P_2 are both on the straight (right-hand) part of the curve, P' will coincide with P_1 and no irreversible flux reduction will be noticed. P' and P'' may be considered as lying on a secondary demagnetization curve that has the knee to the left of P''.

It will be clear now that in many cases it pays to have a construction where the magnet does not work at the $(BH)_{max}$ point, but somewhat higher on the demagnetization curve, where temporary external fields or temporary changes in the air gap do not permanently reduce the useful flux.

When for some reason this is not possible, stabilization is often carried out following the procedure outlined above. In view of these considerations it must be strongly advised that magnets should always be magnetized in their circuits, because magnetization outside the circuit (larger air gap) would automatically result in a lower working point.

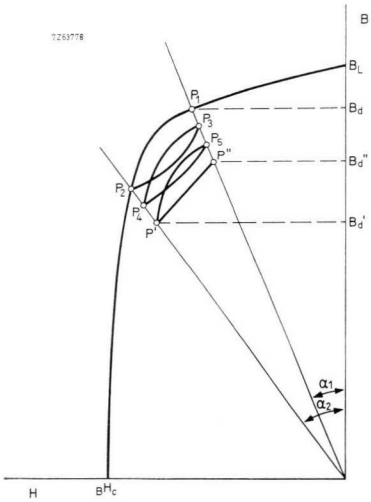

Fig. 6. Shift of load line by changes in the air gap. Stabilization is finally reached in work point P'.

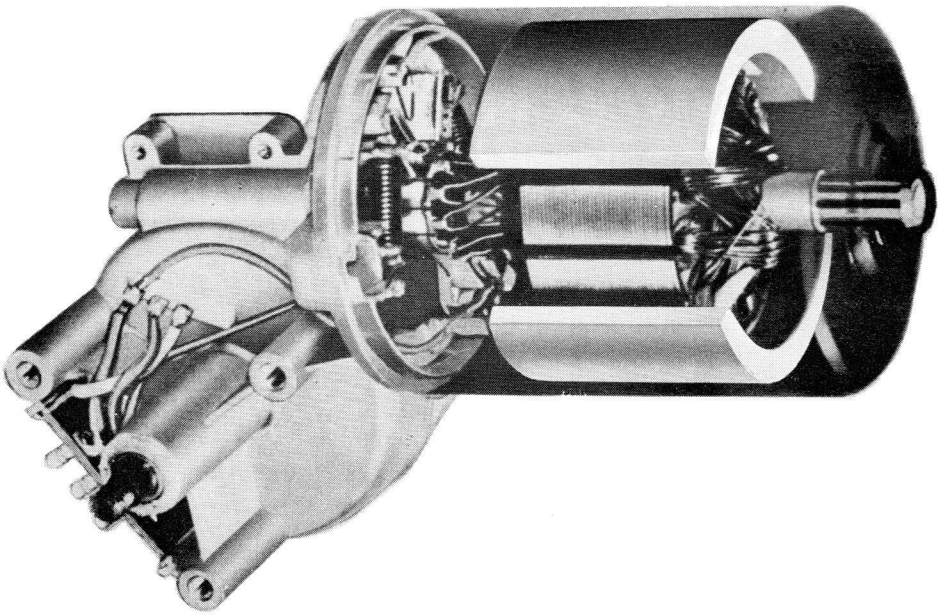

Cut-away vieuw of a two-pole d.c. motor using Ferroxdure segment magnets.
(Courtesy: Fa.Bosch. W. Germany)

This holds for anisotropic Ferroxdure (and for alloy magnets); for isotropic Ferroxdure where the *BH* curve is a straight line down to the *H*-axis, this is not critical as here the working point will nearly always move along the *BH* curve.

Changes in temperature will also alter the position of the working point. This will be dealt with in the following section.

2.8 Temperature Changes in a Magnetic Circuit

The behaviour of Ferroxdure when subjected to changes of temperature is rather complicated, since here we meet two different temperature coefficients and, furthermore, irreversible magnetic changes may occur. The temperature coefficient of the remanence is $-0{,}2\,\%$ per degree Celcius: B_r drops with rising temperature.

That of the coercivity is $+0{,}5\,\%$ per degree, which means that with rising temperature the H_c increases. Fig. 7 shows a set of curves at three different temperatures, -30, $+20$ and $+70\,^\circ$C, for two grades of Ferroxdure. From these figures it can be seen that we have to consider three different magnetic circuits:

1. a circuit with a load line *a*, intersecting all curves in the flat upper part;
2. a circuit with a load line *b*, intersecting all curves in the steep lower part,
3. a circuit that has a load line *c*, intersecting the curves somewhere in the knee.

All three cases will be treated separately. The first case is the easiest: all temperature effects in this area are reversible. A rise in temperature gives a drop in induction and a drop in temperature causes a rise in induction. The variation can easily be calculated from

$$\Delta B = B \cdot TC_{Br} \cdot \Delta T \tag{30}$$

where B is the induction in the magnet or air gap and TC_{Br} the (negative) temperature coefficient, which for temperatures between -30 and $+100\,^\circ$C may be put at $-0{,}2\,\%$ per degree Celcius.

From Fig. 7-I it can be seen that this case is always applicable to the isotropic Ferroxdure 100, since here all *BH* "curves" are straight parallel lines down to the *H*-axis.

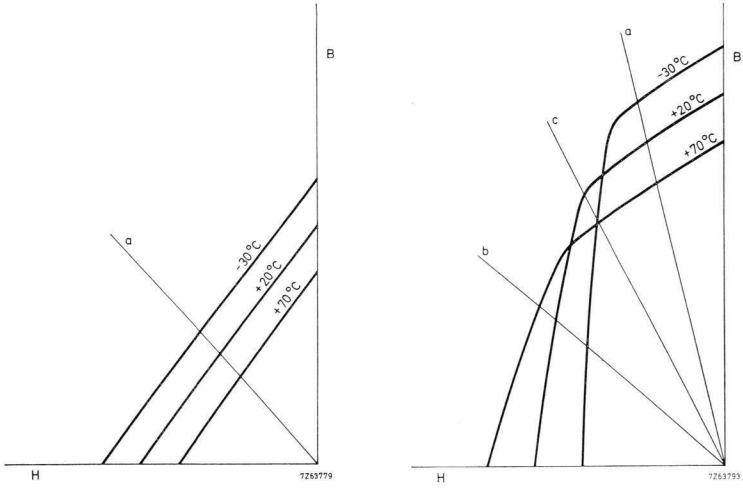

7.I isotropic Ferroxdure 7.II anisotropic Ferroxdure

Fig. 7. Demagnetization curves of Ferroxdure at various temperatures; see text.

For anisotropic Ferroxdure eq. (30) is valid only for circuits with a small air gap (angle α smaller than 23 degrees for FXD300 or 43 degrees for FXD330).

A quite different situation arises when the load line intersects the *BH*-curve in the steep part. Here irreversible changes occur due to internal demagnetization (depolarization). We will not go into the physical background of this phenomenon, but will merely show what happens.

In Fig. 8 two curves, for $+20$ °C and -30 °C respectively, are given for FXD300. Assume a system that is working at point P_1 at $+20$ °C. When this system is cooled to -30 °C the working point will shift to P_2 on the -30 °C curve. Due to internal demagnetization at this temperature and under the specific load angle α the system now acts as when working on a lower imaginary *BH*-curve (dashed line in Fig. 8). When the temperature is raised again the flat part of this curve is displaced due to the negative temperature coefficient. The result seems paradoxical: a raise in temperture causes a further drop of the working point until P_3 is reached, on the dotted line.

The traject P_2-P_3, however, is reversible; if the temperature drops again, the working point will regain P_2. This is graphically depicted in Fig. 8. Of course, all this is without intermediate magnetizing of the system; if resaturation is carried out at 20 °C, point P_1 will immediately be reached again.

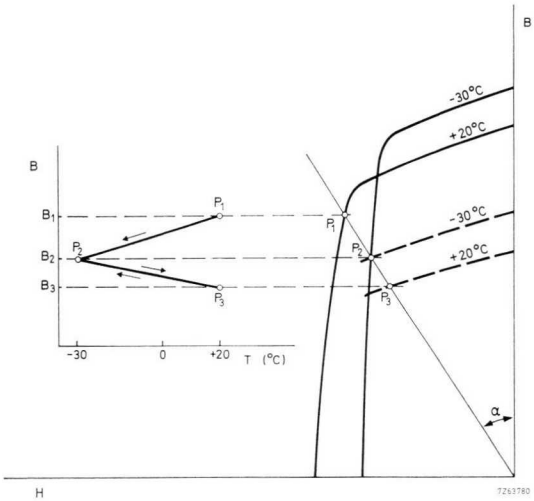

Fig. 8 Influence of temperature variations on a system working below the knee of the demagnetization curve. The first cooling from +20 °C to −30 °C causes a drop in induction from P_1 to P_2. A subsequent rise to +20 °C further decreases the induction to P_3. The system is now stabilized between P_2 and P_3 for temperatures between +20 °C and −30 °C.

The third possibility is the case where the load line intersects the curve in or slightly above the knee, i.e. approximately at the $(BH)_{max}$ point, Fig. 9. Here both a rise and a drop of temperature will cause a drop in the induction. The first is reversible, the second is not. Again a rise in temperature preceded by a drop causes a further drop of the induction which is reversible as explained before.

From all these considerations it will be seen that in order not to suffer from irreversible loss of flux caused by temperature fluctuations, a magnet system should be designed so as to operate well in the upper part of the flat section of the *BH* curve.

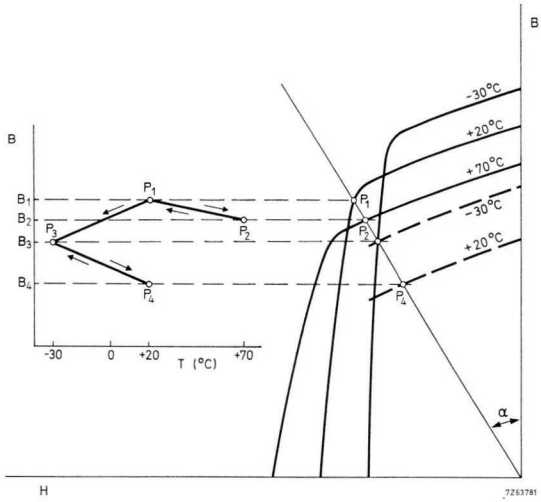

Fig. 9 Influence of temperature changes on a system working in or slightly above the knee of the demagnetization curve. Both a rise and a drop in temperature cause a drop in induction.

Table I gives for various grades of Ferroxdure the maximum values of tan α that are permitted in order to guarantee that no irreversible changes in induction will occur above the indicated temperatures.

This table is valid only if the scale of the graphs is such that 1 division = 1 oersted or, when the SI-system is used, 1 division = 10^{-4} tesla = 79,6 A/m.

If the scale of the graph is 1 division = 10^{-4} tesla = 100 A/m, the values of tan α should be multiplied by a factor 0,796 (= $1/10^5\ \mu_o$).

Table I

FXD	+20 °C	+10 °C	0 °C	−10 °C	−20 °C	−30 °C
260	5,26	3,64	2,63	2,06	1,64	1,33
270	8,10	4,84	3,37	2,52	1,96	1,55
280	1,54	1,29	1,09	0,94	0,82	0,71
300	0,39	0,35	0,32	0,29	0,26	0,24
330	1,32	1,13	0,97	0,84	0,73	0,63
360	0,49	0,45	0,40	0,36	0,32	0,29
370	1,25	1,07	0,92	0,80	0,70	0,60

Symbols used in motor design (chapter 3)

The following symbols are generally used in motor calculations. They are in addition to those already introduced in the first part of this book.

E = e.m.f. of the power supply in volts
E_s = d.c. supply voltage
E_b = voltage drop across 2 brushes
E_i = induced back e.m.f.
I_a = armature current in amperes
M = torque exerted by the motor in newton-metres
R_a = armature resistance in ohms
R_i = internal resistance of the power source in ohms
R_b = brush resistance across 2 brushes
a = number of parallel circuits
n = number of revolutions per second
P = number of poles
z = number of conductors
ϕ = flux in webers
η_e = electrical efficiency factor
η_m = mechanical efficiency factor
N_e = electrical power

3 D.C. Motors with Permanent Magnets

3.1 General

It will be clear that motors with permanent magnet field excitation will necessarily be shunt motors, since the applied field is independent of the armature current.

It is not the aim of this booklet to give a rigorous analysis of this type of d.c. motor. For this we refer to the text books. * We will confine ourselves to recalling a few basic formulae that are in currently use.

The induced back e.m.f. of a d.c. motor is defined as

$$E_i = n\phi \frac{zP}{a} \quad \text{(volts)}. \tag{31}$$

The speed of a d.c. motor is given by

$$n = \frac{E_i}{\phi \dfrac{zP}{a}} = \frac{E_s - I_a R_m}{\phi \dfrac{zP}{a}} \tag{32}$$

where $R_m = R_a + R_b$ = total armature and brush resistance in ohms. Since

$$E_s = E_i + I_a R_b + I_a R_a, \tag{33}$$

the total power $E_s I_a$ consumed by the motor can be divided into two parts, $E_i I_a$ and $I_a R_m$. The latter part represents the ohmic losses in the armature and brushes and consequently $E_i I_a$ stands for the electrical power supplied by the motor, inclusive of losses by friction and eddy currents. So

$$N_e = E_i I_a = n \phi I_a \frac{zP}{a} \tag{34}$$

$$N_e = \text{power in W} \quad \left(= \frac{\text{newton-metres}}{\text{second}} \right).$$

* See e.g. R. Richter, *Elektrische Machinen I*, Birkhäuser Verlag Basel/Stuttgart, and A. E. Fitzgerald and Ch. Kingsley, *Electric Machinery*, McGraw-Hill, New York.

To obtain the torque, N_e should be divided by the angular velocity $2\pi n$, yielding

$$M = \frac{I_a \phi n}{2\pi n} \frac{zP}{a} = \frac{I_a \phi}{2\pi} \frac{zP}{a} \quad \text{(newton-metres).} \tag{35}$$

The electrical efficiency can be expressed as

$$\eta_e = \frac{E_i}{E_s}. \tag{36}$$

The mechanical efficiency η_m depends on frictional (bearings and brushes) and heat losses in the armature laminations. The product $\eta_c \eta_m = \eta_{tot}$ is the overall efficiency. For optimum construction η_c should be about equal to η_m.

For small motors a maximum torque is normally required whereas with larger motors a high efficiency is aimed at.

The following table can be taken as a guide:

motors to 1 W	$\eta_{tot} \approx$ 20 to 40%
1-3 W	up to 50%
3-10 W	up to 60%
over 10 W	60% to 80%.

Generally, the particular application will determine the speed and torque of the motor and the supply voltage. The magnetic circuit of the motor must therefore be designed to produce the value of flux in the air gap necessary for the required speed and torque.

3.2 Magnets in Motors

The required flux can be obtained by using Ferroxdure magnets instead of the orthodox field windings. The magnets can be either in the shape of a ring or of two or more segments. Magnetization can be diametrical or radial.

Radially magnetized rings can only be made of isotropic material; diametrically magnetized ferroxdure rings can be made of both isotropic and anisotropic ferroxdure.

For small motors, say below 1 W, synthetic resin bonded ferroxdure D55 or SP130 may be used.

The value of ϕ in the formulae 31 to 35 depends on the quality of the magnet material, the air gap and the surface area of the magnet segment. For a radially magnetized segment the area A is calculated as

$$A_{rad} = L_s r_i \beta \quad (\mathrm{m}^2) \tag{37}$$

where L_s = axial length in m;
r_i = inner radius in m;
β = angle of segments in radians,
see Fig. 10.

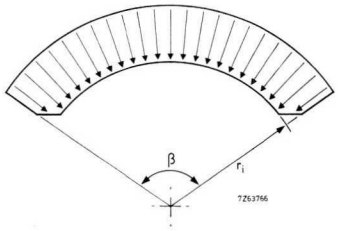

Fig. 10 Radially magnetized segment. Useful area is $A_{rad} = L_s r_i \beta$.

For a diametrically magnetized segment the area should be taken as

$$A_{dia} = 2 L_s r_i \sin \frac{\beta}{2} \quad (\mathrm{m}^2) \tag{38}$$

(for $\beta < 40°$ (37) $\equiv$ (38) within 2%) since here the chord of the segment determines the useful flux, see Fig. 11.

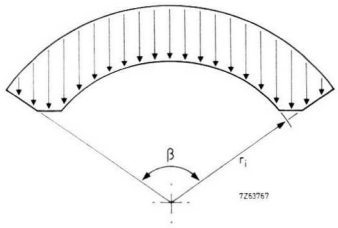

Fig. 11 Diametrically magnetized segment. Useful area $A_{dia} = 2\, L_s r_i \sin \beta/2$.

Since the flux per segment,

$$\phi = B_M \cdot A,$$

the first thing to do is to determine the induction B_M at the working point of the magnet. Eq. (21) gives

$$\frac{B_M}{H_M} = \mu_o \frac{p}{q} \times \frac{A_g}{L_g} \times \frac{L_M}{A_M}. \tag{21}$$

Now the area of the air gap under the magnet segment is virtually the same as the area of the face of the magnet.

So eq. (21) simplifies to

$$\frac{B_M}{H_M} = \mu_o \frac{p}{q} \frac{L_M}{L_g} \tag{39}$$

which can be solved when the characteristics of the magnet material are known. In practice the magnet length should be about 10 times the length of the air gap.

As the total flux per magnet pole is

$$\phi = B_M \cdot A,$$

substitution of eqs (37) and (38) gives

$$\phi = B_M L_s r_i \beta \quad \text{(weber)} \tag{40}$$

for radially magnetized segments, and

$$\phi = B_M \, 2 \, L_s r_i \sin \frac{\beta}{2} \quad \text{(weber)} \tag{41}$$

for diametrically magnetized segments.

The length of the magnet L_M in the actual motor is the radial thickness of the magnet, nominally $(r_o - r_i)$ where r_o and r_i are the outer and inner radii of the segment. The length of the air gap L_g is nominally the difference between the inner radius of the segment and the armature radius plus any gap between the segment outer surface and the stator housing caused by differences in profile.

In practice all these dimensions will have manufacturing tolerances, and allowances must be made for such practical considerations as the eccentricity of the armature and segment radii.

When calculating the flux another point should be taken into account. It usually pays to make the axial lengths of the magnets slightly longer than the axial length of the armature, in order to obtain an increased flux.

Fig. 12 gives a graph of the proportional increase of the flux as a function of L_s/L_A (L_s = axial length of magnet, L_A = axial length of armature) for various values of d_A/L_A (d_A = diameter of armature).

If the magnet is 10% longer than the armature, almost the total flux will go through the armature, in other words $\Delta\phi/\phi$ in Fig. 12 is 10%.

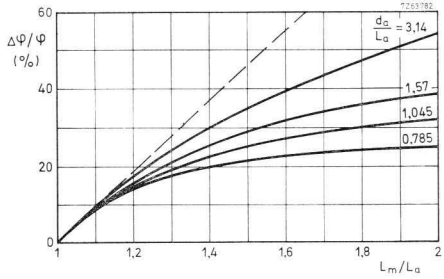

Fig. 12 Increase in useful flux plotted against ratio of magnet to armature length with ratio of armature diameter to length as parameter, L_a is constant.

For larger differences (say $L_s/L_A = 1{,}2$) an extra stray flux of 13 to 17% will occur. In many cases this can be permitted since a saving in armature laminations and copper wire is the result.

It can also be seen from the curves in Fig. 12 that the increase in useful flux is greater for higher values of the ratio of armature diameter to length. Thus this technique of designing motors with the stator magnet longer than the armature is best applied to "flat" armatures (armatures where the axial length is less than the diameter).

3.3 Stator Housing

Since the return of the magnetic flux is through the stator housing that forms the outer body of the motor, the wall thickness of the latter should be such that magnetic saturation does not occur. To ensure that the magnetic losses are kept within reasonable limits, it is necessary to keep the flux density in the return path to less than 1,5 tesla. This means that the minimum cross-sectional area of the return path is given by:

$$A_{rp} = \frac{\phi}{1{,}5\,p} \quad (\mathrm{m}^2)$$

where p = the number of poles of the motor.

Taking L_s as the axial length of the magnet this yields a wall thickness of the housing of

$$T_W = \frac{\phi}{L_s\,p\,1{,}5} \text{ metres.} \tag{42}$$

3.4 Designing a Permanent Magnet Motor

The parameters indicated by the symbols on page 24 are by no means complete. There are still more points to consider when designing a motor. The number of wires calculated should be accommodated in the available or possible number of slots: the "filling factor" should be lower than 0,3. The heat dissipation also has to be considered. If the heat generated in the armature windings cannot be conducted away and removed through the armature surface, the motor insulation will deteriorate from excessive heating.

A third point is the sensitivity to low and high ambient temperatures; sometimes the torque is specified at −30 °C.

In order to be able to design the optimum motor we have set up a computer program into which all variables can be fed. Some parameters will be exactly specified, such as voltage, torque, diameter, speed, whereas of others only limits will be given.

Following a reiterative method, it is now possible to convert an existing wound field motor into a Ferroxdure motor, or to design an entirely new motor in a very short time.

By inserting the prices of ferroxdure, copper, iron laminations and housing in the computer program, it will eventually be possible to select the most economic solution from various versions.

Nevertheless to make the reader acquainted with the general procedure we will give a detailed example of the calculations for a specific motor. The general performance characteristics of a permanent magnet d.c. motor are shown in Fig. 13. The optimum operating speed for the motor is ω_w, the speed for maximum efficiency. However, motors are also designed to operate at maximum power, or for some compromise between power and efficiency.

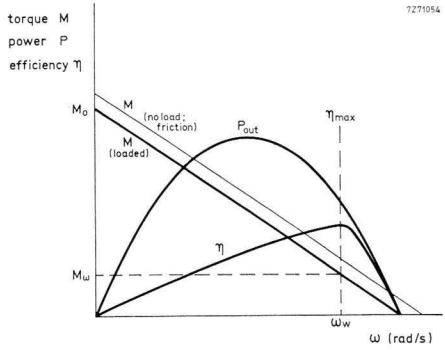

Fig. 13 General performance characteristics of a permanent magnet d.c. motor.

Assume a motor is required with the following specification:

$E = 14$ V ;
starting torque $M_o = 70 \times 10^{-2}$ Nm;
torque at 50 rev./s $M_{50} = 9 \times 10^{-2}$ Nm;
diameter of armature $D_a = 41 \times 10^{-3}$ m;
number of slots in armature: 10,
cross-section of slots: 40×10^{-6} m^2.

Furthermore the motor should have two poles and two parallel circuits:
$P = 2$ and $a = 2$.

The values of $z\phi$ and R_{tot} $(= R_i + R_a + R_b)$ can be calculated from eqs (31), (33) and (35).

Substitution of eq. (31) in eq. (33) yields:

$$E = I_a R_i = n \frac{P}{a} z\phi + I_a R_a + I_a R_b \text{ where } I_a = \frac{E - \left(n \frac{P}{a} z\phi + E_b\right)}{R_a + R_i}. \tag{43}$$

This inserted in eq. (35) gives

$$M = \frac{1}{2\pi} \cdot \frac{P}{a} z\phi \frac{E - \left(n \frac{P}{a} z\phi + E_b\right)}{R_a + R_i} =$$

$$= \frac{1}{2\pi (R_a + R_i)} \left\{ (E - E_b) \frac{P}{a} z\phi - \left(\frac{P}{a} z\phi\right)^2 n \right\}. \tag{44}$$

At $n = 0$ the mechanical efficiency coefficient will be 1. We furthermore assume that the motor will be fed by an accumulator having an internal resistance of 0,01 Ω and that the total voltage drop across the brushes is 0,6 V.

Eq. (44) then yields:

$$M = \frac{M_o}{\eta_m} = \frac{70 \times 10^{-2}}{1} = \frac{1}{2\pi (R_a + R_i)} \{(14 - 0{,}6)\, z\phi\}$$

$$R_a + R_i = \frac{13{,}4}{2\pi \times 70 \times 10^{-2}} z\phi. \tag{45}$$

At 50 rev./s η_m will be about 0,8. Eq. (44) yields

$$M_e = \frac{M_{50}}{\eta_m} = \frac{9 \times 10^{-2}}{0{,}8} = \frac{1}{2\pi (R_a + R_i)} \{(14 - 0{,}6)\, z\phi - 50\, (z\phi)^2\}$$

or

$$9 \times 10^{-2} \times 2\pi (R_a + R_i) = 0{,}8\, \{13{,}4\, z\phi - 50\, (z\phi)^2\}. \tag{46}$$

Substituting eq. (45) in eq. (46) we find:

$z\phi = 0{,}225$ Wb × number of conductors.

And consequently:

$$\boldsymbol{R_a + R_i = 0{,}677\,\Omega}$$

$$\boldsymbol{R_a = 0{,}667\,\Omega}$$

The current at 50 revolutions per second can now be calculated from the formula

$$E - I_a R_i = E_b + E_i + I_a R_a$$

$$14 - 0{,}01\, I_a = 0{,}6 + 50 \times 0{,}225 + 0{,}667\, I_a$$

$$\boldsymbol{I_a = 3{,}18\,\mathrm{A}.}$$

The electrical efficiency will be

$$\eta_e = \frac{E_i}{E - I_a R_i} = \frac{50 \times 0{,}225}{14 - 3{,}18 \times 0{,}01} = 0{,}805,$$

giving an overall efficiency of

$$\eta_{tot} = \eta_m \times \eta_o = 0{,}8 \times 0{,}805 = 0{,}644.$$

Taking into account an air gap of length 0,5 mm, the internal diameter of the segments should be $(0{,}041 + 2 \times 0{,}005) = 4{,}2 \times 10^{-2}$ m. If we take two segments of 7 mm thickness, the outer diameter of the segments will be $(42 + 2 \times 7)$ mm $= 5{,}6 \times 10^{-2}$ m.

We chose a segment of FXD280 with an angle of 140° (2,44 radians) and can now calculate the flux yielded per unit of axial length. This flux can easily be found since we are working in the linear part of the demagnetization curve. To increase the useful flux an overhang of 30% is taken which, as can be seen from Fig. 12, gives a 20% rise in flux.

$$\phi = B_M A_M \times 1{,}2 \times 10^{-4} \quad \text{(Wb/cm length).}$$

B_M, the induction in the magnet at the working point can be determined with the aid of eq. (21).

$$\frac{B_M}{H_M} = \mu_o \frac{p}{q} \times \frac{L_M}{L_g} \times \frac{A_g}{A_M}. \tag{21}$$

We assume p and q to be equal to 1 and the area of the magnet equal to the area of the gap.

Eq. (21) changes into:

$$\frac{B_M}{H_M} = \mu_o \frac{L_M}{L_g} = 4 \times \pi \times 10^{-7} \frac{7 \times 10^{-3}}{0{,}5 \times 10^{-3}} = 176 \times 10^{-7}.$$

This represents the static load of the magnet, that can be plotted in the demagnetization curves of FXD280, see Fig. 14.

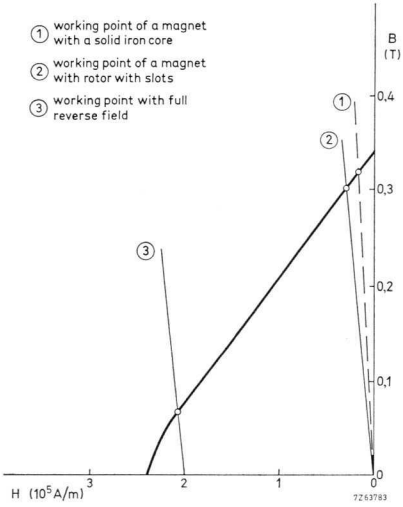

Fig. 14 Demagnetization curve of ferroxdure 280 with
1. static load line for system with a solid iron core;
2. static load line for actual motor with slotted armature,
3. permitted reverse field at room temperature.

From this graph we can now read the working point to be at 0,317 tesla.

It has been found empirically that when we do not have a solid iron core, but a grooved core, as is the case here, a decrease of 5% in B_M is to be expected. So the real B_M will be $0{,}95 \times 0{,}317 = 0{,}301$ T. The load line pertaining to this B_M is also shown in Fig. 14.

The flux can now be calculated:

$$\phi = 0{,}301 \times 2{,}1 \times 2{,}44 \times 1{,}2 \times 10^{-4} = 1{,}86 \times 10^{-4} \quad \text{(Wb/cm axial length).}$$

From the value of $z\phi = 0{,}255$ found earlier we can calculate the number of conductors as a function of the axial length of the armature:

$$L_A = 1 \times 10^{-2} \text{ m} \qquad \phi = 1{,}86 \times 10^{-4} \text{ Wb} \qquad z = \frac{0{,}225}{1{,}86 \times 10^{-4}} = 1210.$$

$$L_A = 2 \times 10^{-2} \text{ m} \qquad \phi = 3{,}72 \times 10^{-4} \text{ Wb} \qquad z = 605.$$

$$L_A = 3 \times 10^{-2} \text{ m} \qquad \phi = 5{,}58 \times 10^{-4} \text{ Wb} \qquad z = 403.$$

$$L_A = 4 \times 10^{-2} \text{ m} \qquad \phi = 7{,}44 \times 10^{-4} \text{ Wb} \qquad z = 302.$$

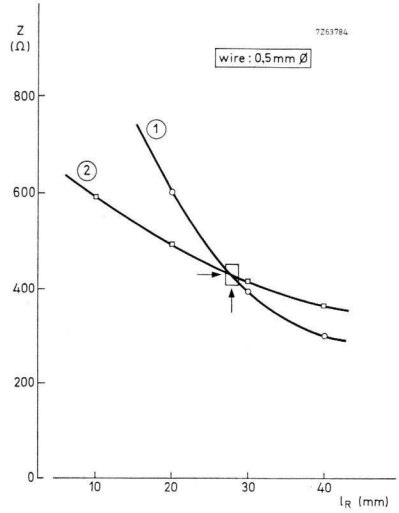

Fig. 15 Number of conductors, z, plotted against the axial length of the segment.
1. as calculated from $z\phi$,
2. as calculated from the armature resistance R_a.

These values have been plotted in Fig. 15. A permissible current density S_A for copper wire is approximately 8 A/mm². The required copper cross-section is consequently

$$\frac{I_a}{a\,S_a} = \frac{3{,}18}{2{,}8} = 0{,}199 \text{ mm}^2 = 0{,}199 \times 10^{-6} \text{ m}^2.$$

A commercially available wire size is 0,5 mm with a cross-section of $0{,}1965 \times 10^{-6}$ m² and an electric resistance of 0,088 Ω/m. The value of z can now also be calculated from R_a. The formula is

$$R_a = \frac{\text{length per conductor} \times z \times 0{,}088}{a^2}.$$

The length of one conductor is taken as the sum of the armature length and the armature diameter:

$$R_a = \frac{(L_a + D_a) \times Z \times 0{,}088}{a^2},$$

$$z = \frac{R_a a^2}{0{,}088\,(L_a + D_a)}$$

$$z = \frac{0{,}0667 \times 4}{0{,}088\,(L_a + 4{,}1)}$$

This gives:

$L_A = 1 \times 10^{-2}$ m	$z = 594.$
$L_A = 2 \times 10^{-2}$ m	$z = 496.$
$L_A = 3 \times 10^{-2}$ m	$z = 417.$
$L_A = 4 \times 10^{-2}$ m	$z = 374.$

These values were also plotted in Fig. 15. It is evident that the point of intersection of the curves will be the best compromise. So an armature of 28 mm length with a total number of 440 conductors, i.e. 220 turns, should meet the requirements.

For 10 slots this means 44 wires per slot or 22 turns per coil. The total cross-section area of these wires is $44 \times 0{,}1965 \times 10^{-6}$ m² $= 8{,}65 \times 10^{-6}$ m². The area of the slot is 40×10^{-6} m², so the filling factor $40/8{,}65 = 0{,}216$ which is an acceptable value.

The electric losses in the armature are $I_a^2 R_a = 3{,}18^2 \times 0{,}667 = 6{,}78$ W, which are to be dissipated through the cooling surface of the armature. This has an area of $\pi D_a I_a = \pi \times 4{,}1 \times 2{,}8 \times 10^{-4}$ m^2 $= 36 \times 10^{-4}$ m^2.

In practice the specific heat transfer is $6{,}78/36 \times 10^{-4} = 0{,}188 \times 10^4$ W/m^2, a permissible value, in view of the rise in temperature of the motor.

The induced reverse field in the motor can be calculated with the formula

$$H_i = \frac{\dfrac{I_o}{a} \cdot z \dfrac{\alpha}{2\pi}}{2(L_M + L_g)},$$

where I_o, the current within the motor, is

$$\frac{E - E_b}{R_a + R_i} = \frac{13{,}4}{0{,}677} = 20 \text{ A}.$$

So

$$H_i = \frac{\dfrac{20}{2} \times 440 \times \dfrac{2{,}44}{2\pi}}{2\,(0{,}7 + 0{,}05)10^{-2}} = 112 \times 10^3 \text{ A/m}.$$

From the demagnetization curve of FXD280 it can be seen (Fig. 15) that a field of 186×10^3 A/m is permitted at room temperature, so no permanent demagnetization will occur at start.

At lower temperatures the permitted reverse field is lower, as can be seen from Fig. 16, where the demagnetization curves of FXD280 at lower temperatures are partially shown.

Table II shows the permitted reverse field together with the induced reverse field at various temperatures.

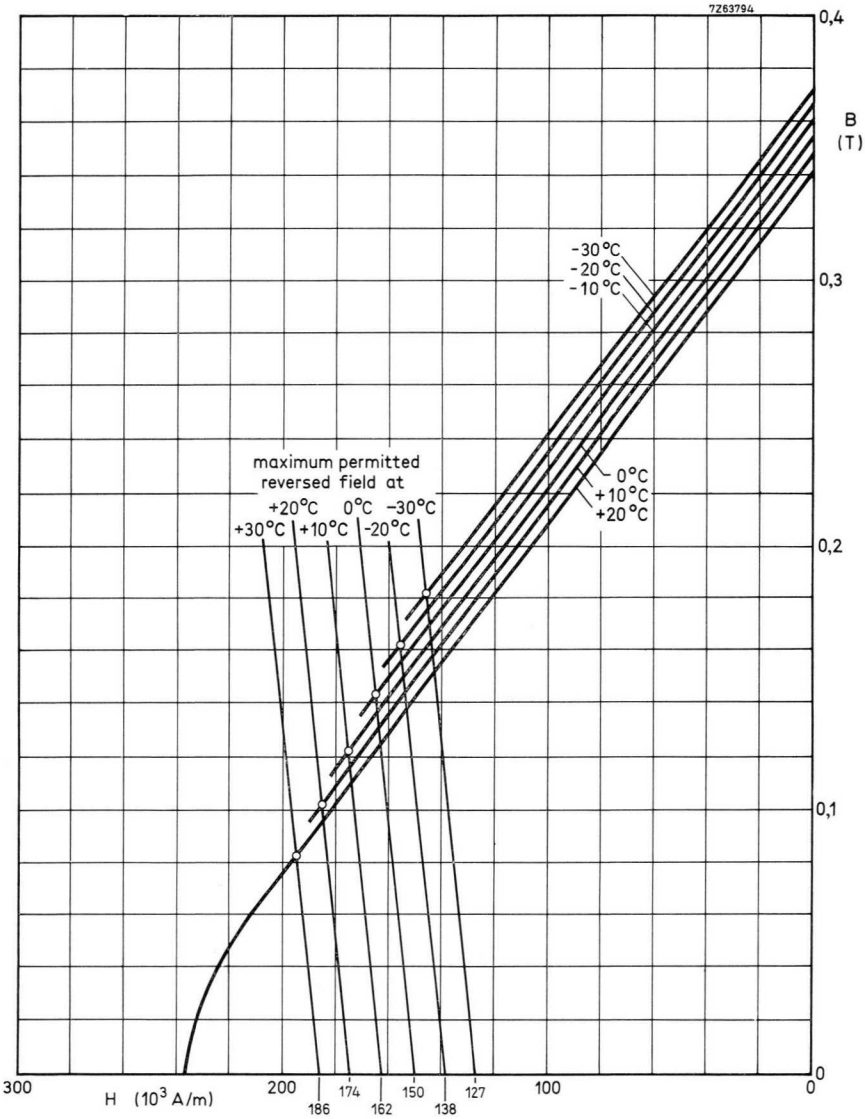

Fig. 16 Permitted reverse field at temperatures down to −30 °C.

Table II

temperature °C	permitted reverse field A/m	induced reverse field A/m
+20	186×10^3	112×10^3
+10	174×10^3	115×10^3
0	162×10^3	120×10^3
−10	150×10^3	125×10^3
−20	138×10^3	$130{,}5 \times 10^3$
−30	127×10^3	$136{,}5 \times 10^3$

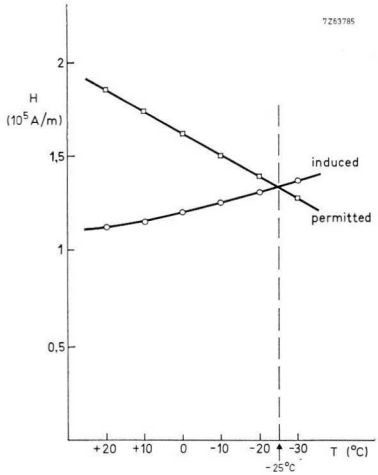

Fig. 17 Permitted and induced reverse fields plotted as a function of temperature. The motor is stable down to −25 °C.

Both permitted and induced reverse field are plotted in Fig. 17 as a function of temperature. The intersection of the two graphs is at −25 °C, which means that the motor will be stable down to that temperature.

Since the return flux through the armature passes through the housing, the thickness of this should be such that no saturation will occur.

The flux from the segments is

$$\phi = \frac{z\phi}{z} = \frac{0{,}225}{440} = 5{,}1 \times 10^{-4} \text{ Wb.}$$

If the length of the housing is equal to the length of the segments, i.e. 1,33 times the length of the armature, eq. (42) yields

$$T = \frac{5 \times 1{,}0^{-4}}{1{,}33 \times 28 \times 10^{-3} \times 2 \times 1{,}5} = 0{,}45 \times 10^{-2} \text{ m.}$$

The total diameter of the motor will be

$$\begin{aligned} D_M &= D_a + 2L_g + 2L_M + 2T \\ &= 0{,}041 + 0{,}001 + 0{,}014 + 0{,}009 \text{ m} = 0{,}065 \text{ m} = 65 \text{ mm.} \end{aligned}$$

Although this example illustrates the design method, it should be noted that it will usually be necessary to repeat the procedure several times before a design is evolved which satisfies all requirements. This necessary repetition is incorporated in the computer program already mentioned.

3.5 Multipole motor design

The practical design considerations given so far have referred only to the 2-pole motor, despite the fact that the general discussion of section 3.1 included the number of poles, P, as a variable. From the discussion and from Eqs (31) to (36), it will be apparent that there are certain definite advantages to be obtained from using a larger number of poles.

These advantages may be summarized briefly. In Fig. 14, the various demagnetization allowances have been plotted. By far the largest demagnetizing influence which has been allowed for is that due to the armature. Now, on any one pole, the reverse field generated by any given armature depends on the proportion of the armature which the pole covers. Since the product $z\phi$ must remain constant for any given performance motor, Eq. 31, the demagnetization to be allowed for must depend on the number of poles used. Thus with four poles, half the reverse field will be encountered by the ferrite than with two poles, and so on with six, eight and more poles. Reduction of the reverse field reduces magnet length and, therefore, volume required.

A second important effect of increasing the number of poles is that the peak level of flux to be carried by the stator housing is reduced. This peak occurs at the edge of each magnet, and in a 2-pole motor amounts to one quarter of the total motor flux ϕ. So, with a 4-pole motor, the peak flux level to be carried by the stator housing becomes one eighth of the total, and the flux density and thus the cross section of the housing is halved.

There are inevitably some limitations to the extent of the advantage to be obtained from increasing the number of poles in this way. Firstly, the minimum housing thickness for any given motor will usually be set by mechanical strength requirements. Secondly, very thin ferroxdure segments may be too brittle to be handled without breakage. Also the commutator resolution will set a further limit. Advantages to be gained from material weight reduction will eventually be offset by the increasing processing costs of a greater number of piece-parts.

Finally, magnetizing and testing costs increase with the number of poles involved.

Most of the above limitations imply a scale effect. The advantages from increasing the number of poles become greater as the size of the motor, and, particularly, the weight of materials in the stator increase. A definite advantage is to be found in going to a four-pole construction for larger motors. In one design comparison, for a 3/4 h.p. (560 W) motor, the 4-pole version was 35% lighter than the 2-pole equivalent. The 2- and 4-pole versions of the motor are compared in Fig. 18.

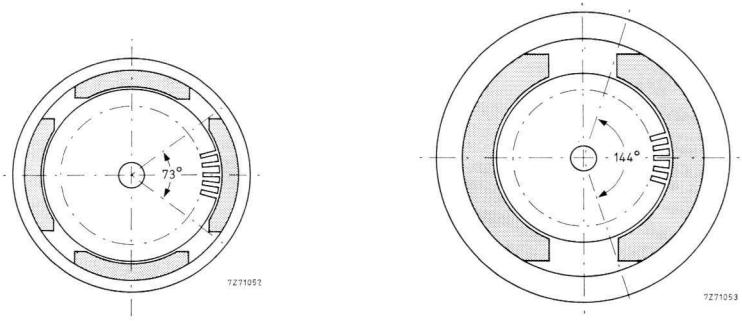

(*a*) (*b*)

Fig. 18. Cross-section through a 2-pole (a) and a 4-pole (b) motor of the same performance. The reduction of material used in the 4-pole version is evident.

4 Dimensions and Tolerances of Magnets for D.C. Motors

The motor manufacturer's requirements for stator-field magnets for use in d.c. motors can be summarized as follows:

1. the magnet should produce the required value of gap flux for the specified operating conditions of the motor;
2. the magnets must be capable of being assembled with the other components of the motor to form a satisfactory unit.

The first requirement is met by the magnetic inspection of the finished magnets. The second requirement involves the correct tolerances on certain dimensions of the magnet, together with those of associated components, to ensure that under all conditions of component tolerances a satisfactory motor can be assembled.

Because segment magnets are a form not easily checked by conventional measurements the emphasis will be laid on gauging. Since the dimensions of armature and stator housing are known, the dimensions of the magnet segment must be chosen so as to allow correct fitting in the space available. This is shown in Fig. 19. If the outer radius of the segment were to be smaller than the inner radius of the housing, the segment would touch the housing at the mid-point only and would therefore rock. This would obviously be undesirable. The segment should touch the housing at two points, which means that the minimum

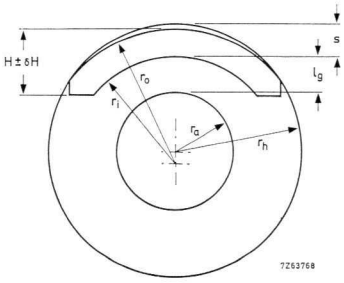

Fig. 19 Cross-section of segment magnet in stator housing. The gap between the segment and housing has been exaggerated for clarity.

outer radius of the segment must be larger than the maximum inside radius of the housing:

$$r_{o\ min} \nless r_{h\ max}.$$

The minimum inner radius of the segment should be equal to the sum of the armature radius plus the length of the air gap with an extra allowance for for eccentricity of say 0,1 mm:

$$r_{i\ min} \nless r_{a\ max} + L_g + 0{,}1 \text{ mm}.$$

In order to make the magnet fit into the housing, dimension in Fig. 19 should be equal to or smaller than the difference between the minimum radius of the house and the minimum calculated inner segment-radius.

When the magnets are to be retained in the housing by means of springs between the flat ends, dimension H with its tolerance δH is important. From the above it will be clear that the best method to check the essential dimensions is by gauging. Two gauges are used, a "GO" gauge and a "NO GO" gauge.

The "GO" gauge is shown in Fig. 20. It defines the maximum space that the segment may occupy, consisting of two concentric arcs of radii $r_{h\ min}$ and $r_{a\ max} + L_g + 0{,}1$ mm respectively, cut by a chord at a distance of $r_{h\ min} - (H + \delta H)$ from the centre of curvature of the two arcs. The segment magnet should pass through the segment cut-out in the gauge.

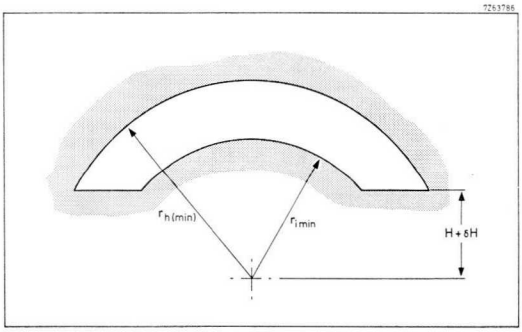

Fig. 20 GO-gauge for segment magnets.

The "NO GO" gauge is shown in Fig. 21. It consists of an arc of radius $r_{h\,min}$ cut by a chord at a distance $r_{h\,min} - (H - \delta H)$ from the centre of curvature. The segment magnet should not be able to pass through this aperture. It can be seen, that this simple method of checking that a segment will pass through one gauge but not through a second, ensures that segments are supplied satisfying the requirement that any two or more segments can be assembled into a motor without special selection.

The dimensions of ring magnets can easily be checked with a calliper gauge. Here the outer radius should be smaller than the minimum radius of the housing:

$$r_o \ngtr r_{h\,min}.$$

The inner radius should be larger than or equal to the sum of the maximum radius of the armature and the air gap, increased by 0,1 mm for eccentricity.

$$r_i \ngtr r_{a\,max} + L_g + 0{,}1 \text{ mm}.$$

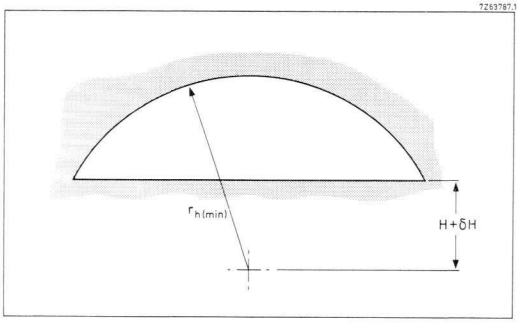

Fig. 21 NO GO-gauge for segment magnets.

5 Magnetization and Demagnetization

5.1 Equipment for Generating Magnetization Currents

Magnetization and demagnetization of magnets and magnetic systems require high strength magnetic fields which are produced by electromagnets. In general it may be said that the internal field H required in ceramic permanent magnetic materials should be about three times as strong as the coercivity field of magnetic polarization (${}_IH_c$).

The relationship between the external field (H_{ext}) and the inner field is expressed as

$$H_{ext} = H + N_{de}M$$

where M is magnetization, and hence depends on the demagnetization factor N_{de} of the part concerned. In this section only external field strengths are calculated.

Whereas the variation of the external field is proportional to the energizing current, the power loss varies as the square of the current. Therefore magnetizing equipments were designed which would produce the required field strengths with the lowest possible losses. Such equipments are current pulse generators, in which the pulse duration, and therefore energy used, is kept as small as possible. for the application.

There are four methods of generating current pulses:

1. from the mains via a rectifier;
2. from the mains via a switching device (ignitrons or thyristors);
3. from the mains via a capacitor discharge,
4. from a d.c. supply via an inductance.

Pulse generators belonging to the groups 1 and 2 operate without a buffer and draw the power required directly from the mains at a pre-set timing. This imposes a considerable load on the mains and, hence, calls for a powerful installation. Pulse generators of group 3 draw the magnetizing power from charged capacitors. The discharge takes place in 1 to 10 milliseconds, whilst a re-charge takes 1 to 10 seconds. As a result the load on the mains is reduced by a factor of 1000. These types of equipment can usually be connected to a 220 V, 15 A mains. Pulse generators of group 4 require a d.c. mains or generator.

5.1.1 D.C.-MAGNETIZATION EQUIPMENT

Fig. 22 gives the circuit diagram of a magnetization apparatus with rectifier connected. R and L in the diagram represent the resistance and the inductance of the magnetizing coil respectively. Of course, a strong current supplied by a d.c. generator could also be used for the same purpose. But since such high currents are usually not ready at hand and, moreover, require special switchgear, the circuit of Fig. 22 is preferred. Note that the switch should be connected on the mains side.

If the internal resistance of the power supply is low compared with the resistance of the magnetizing coil, the current will be about

$$I = \frac{V}{R}(1 - e^{-t\,R/L}). \tag{47}$$

The maximum current, limited by the terminal voltage and the resistance of the coil, is obtained only after the current surge has reached its maximum value. Hence, equipment operating on this principle is not suitable for obtaining variable short pulse durations.

5.1.2 HALF CYCLE MAGNETIZERS

Fig. 23 gives the circuit diagram of a half-cycle magnetizer. When the ignitron is made conductive, a current will begin to flow through the coil. A current of opposite direction is blocked by the ignitron, so that this type of equipment utilizes half-cycles of the mains.

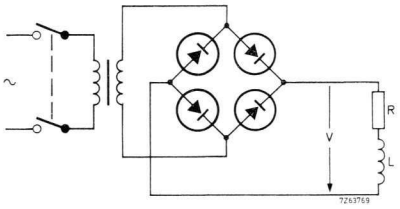

Fig. 22 Circuit of a d.c. magnetizer.

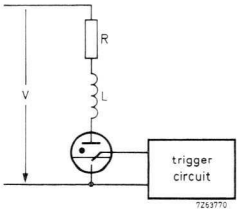

Fig. 23 Circuit of a half-cycle magnetizer.

If the ignitron is triggered at the moment the a.c. changes sign, or passes zero, the current during the first half-cycle, as calculated from the switch-on conditions is

$$I_{(t)} = \frac{V_{peak}}{\sqrt{(R^2 + \omega^2 L^2)}} \{\sin(\omega t - \phi) + \sin\phi\, e^{-t\,R/L}\} \tag{48}$$

with

$$\tan\phi = \frac{\omega L}{R} \tag{49}$$

(V_{peak} = peak voltage, ω = angular frequency).

The conditions for maximum current, I_{max}, are found from the equation

$$\cos(\omega t - \phi) = \cos\phi 2^{-\omega t \cot\phi}. \tag{50}$$

For a given value of ϕ, eq. (50) can be used to find ωt, which in turn can be inserted in eq. (48) to calculate the maximum current.

It is impossible to give an exact formula for calculating the maximum current I_{max} (as a function of ϕ).

It is found, however, that at this maximum,

$$\omega t \approx \frac{\pi}{2} + \phi. \tag{50a}$$

This formula inserted in eq. (48) gives a useful formula which yields values over the total range $0 < \phi < \pi/2$ with an error of no more than 1%:

$$I_{max} = \frac{V_{peak}}{\sqrt{(R^2 + \omega^2 L^2)}} \{1 + \sin\phi\, e^{-(\pi/2+\phi)\cot\phi}\}. \tag{51}$$

For $\phi = 0$ (i.e. $R \gg \omega L$) and $\phi = \pi/2$ (i.e. $R \ll \omega L$) this formula is exact. We then find

$$I_{max} = \frac{V_{peak}}{R} \tag{52}$$

and

$$I_{max} = \frac{2V_{peak}}{\omega L}. \tag{52a}$$

In Fig. 24 the maximum current obtained at the peak voltage is plotted against the coil inductance with the coil resistance as a parameter. At inductances $> 0{,}1$ H and coil resistance $< 10\ \Omega$ the inductance value is the main current determining factor, whilst at inductances $< 10^{-3}$ H the current depends mainly on the coil resistance.

5.1.3 Capacitor Discharge Magnetizers

Fig. 25 shows the circuit diagram of a capacitor discharge magnetizer. The charged capacitor C is an energy buffer which discharges across the coil as soon as the ignitron fires. Even if the coil is so dimensioned that damped oscillation can occur, the ignitron only permits a current half-cycle to flow through the coil.

For magnetizing only the maximum current is of interest. If the conditions for damped oscillation are present, i.e. if:

$$\frac{R}{2} < \sqrt{\frac{L}{C}}, \tag{53}$$

the maximum current can be expressed as:

$$I_{max} = V_o \sqrt{\frac{C}{L}} \exp\left\{ -\frac{\arctan \sqrt{\left(\frac{4L}{R^2C} - 1\right)}}{\sqrt{\left(\frac{4L}{R^2C} - 1\right)}} \right\}. \tag{54}$$

where V_o is the initial voltage across the capacitor. This expression may be approximated to:

$$I_{max} = V_o \sqrt{\left\{ \frac{C}{L} e^{-R/2 \sqrt{(C/L)}} \right\}} \tag{54a}$$

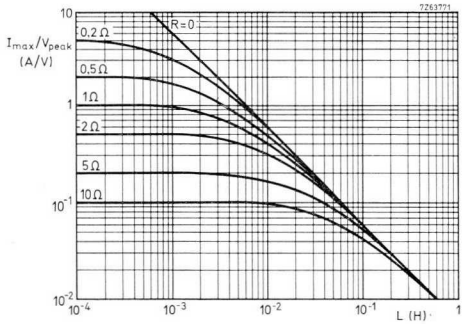

Fig. 24 Maximum current at peak voltage plotted against coil inductance with the copper resistance as parameter.

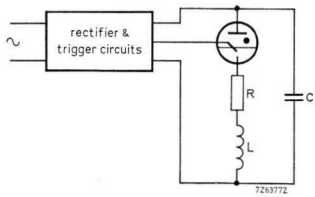

Fig. 25 Circuit diagram of a capacitor discharge magnetizer.

All deviations resulting from using this formula remain below $+12\%$. For $R = 0$ (undamped oscillation) eq. (54) can be simplified to

$$I_{max} = V_o \sqrt{\frac{C}{L}} \tag{54b}$$

which also follows from the requirement for equal (maximum) electric and magnetic energy:

$$\tfrac{1}{2} C V_o^2 = \tfrac{1}{2} L I_{max}^2. \tag{55}$$

For the aperiodic border case, i.e.

$$\frac{R}{2} = \sqrt{\frac{L}{C}} \tag{56}$$

the maximum current can be written as

$$I_{max} = V_o \sqrt{\frac{C}{L}}\, e^{-1} \tag{54c}$$

and for the aperiodic general case, as

$$\frac{R}{2} > \sqrt{\frac{L}{C}}\,. \tag{57}$$

We finally find:

$$I_{max} = V_o \sqrt{\frac{C}{L}} \exp\left\{ -\frac{\operatorname{arctanh} \sqrt{\left(1 - \frac{4L}{CR^2}\right)}}{\sqrt{\left(1 - \frac{4L}{CR^2}\right)}} \right\} =$$

$$= V_o \sqrt{\frac{C}{L}} \left\{ \frac{1 - \sqrt{\left(1 - \frac{4L}{CR^2}\right)}}{1 + \sqrt{\left(1 - \frac{4L}{CR^2}\right)}} \right\}^{\left[2\sqrt{\left(1 - \frac{4L}{CR^2}\right)}\right]^{-1}} \tag{54d}$$

Fig. 26 shows the maximum pulse current for a capacitor discharge magnetizer as a function of the inductance L for different values of the coil resistance R. The capacitor has a value of 1400 μF; the initial voltage $V_o = 1000$ V.

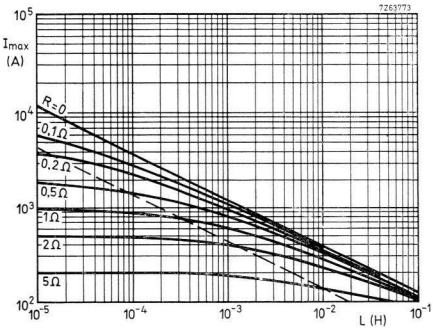

Fig. 26 Maximum pulse current for a capacitor discharge magnetizer as a function of the inductance L, with the coil resistance as a parameter.

The dashed straight line in the plot applies to the aperiodic border case: the area to the right of the line concerns damped oscillations, the area to the left relates to the aperiodic case. To obtain a high field strength, the product $N\,I_{max}$ must be as high as possible (N is the number of turns). It is, therefore essential that R is very low and that the equipment operates practically within the range of undamped oscillations. In that case the switching time, which covers half a cycle is found as

$$t = \frac{\pi}{\sqrt{\left(\frac{1}{LC} - \frac{R^2}{(ZL)^2}\right)}} \tag{58}$$

or for

$$\sqrt{\frac{L}{C}} \gg \frac{R}{2}, \qquad t = \pi\sqrt{(LC)}. \tag{58a}$$

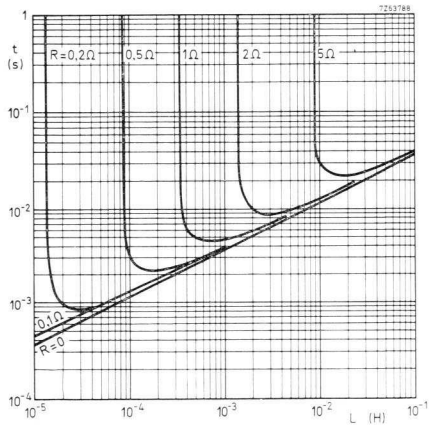

Fig. 27 Switching time of a capacitor discharge magnetizer as a function of the coil inductance, with the coil resistance as a parameter. (Initial voltage $V_0 = 1000$ V, $C = 1400$ μF.)

The switching times calculated with eq. (58) can be read from Fig. 27. The value of the capacitor was again chosen as $C = 1400$ μF. For

$$L = \frac{CR^2}{2} \tag{59}$$

the switching on time reaches a minimum:

$$t = 2\pi \frac{L}{R} \tag{60}$$

and depends only on the dimensions of the coil.

5.1.4 Pulse Transformers

Pulse transformers are also a form of magnetizing equipment with an energy buffer. For technical and economical reasons this method of current pulse generation for magnetizing is now seldom used. However, for completeness' sake it is discussed here.

The primary winding of the pulse transformer is fed with a direct current. The secondary winding, consisting of only a few turns, is shorted via the magnetizing circuit (e.g. a bar or a coil of only a single turn). As soon as the energizing direct current is switched off, the magnetic field energy will flow away through the secondary winding. The current pulse thus produced is used for magnetizing. To obtain the right amount of magnetic power, heavy and bulky equipment must be made which, particularly owing to the amount of copper needed, is quite expensive.

To reduce this cost, low induction and low loss magnetizing coils are used, even a straight conductor with soft iron yoke or a one turn coil. So the forms and dimensions of the magnetizing coils are subject to considerable limitation. Further disadvantages are that the primary of the transformer must be energized with a direct current which is not always readily available and even if it is, involves switching problems. This is also the reason why such equipment is unsuitable for achieving a high production rate.

5.2 Coils for Magnetizing Rings and Segments for D.C. Motors

Magnetizing of these rings or segments can take place before or after insertion in the housing. In mass production it is more efficient to magnetize after insertion in the housing because it is so much easier to remove swarf and small magnetic particles prior to magnetizing. After magnetizing, the motor is assembled, after which the magnets are protected against mechanical damage. One method of magnetizing the stator from the inside will be described.
sembled, after which the magnets are protected against mechanical damage. One method of magnetizing the stator from the inside will be described.

The basic construction of a coil for magnetizing magnets in d.c. motors is shown in Fig. 28. The inner space filled by the armature when the motor is complete is now available to receive the magnetizing coil. The soft iron core should preferably be made of laminated cold rolled sheet steel, and here too the winding should lie properly insulated in the grooves. To immobilize the windings and to improve heat removal it the use of a potting resin is recommended. For bi-polar magnetizing the winding encirles practically the whole cross-section of the soft iron armature. Armature dimensions of about 50 mm require up to 30 turns: owing to its high filling factor and the associated good heat removal, square section wire (e.g. 1×7 EnCu) is particularly suitable. As inductions from 1,2 to 1,4 tesla are required for magnetizing Ferroxdure magnets, it is useful to check the induction in the soft iron core. The magnetizing flux ϕ_M in the magnet is

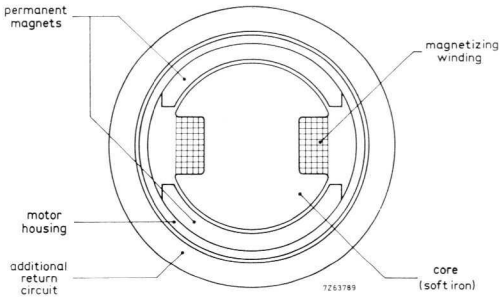

Fig. 28 Magnetizing coil for ring or segments in the motor housing.

$$\phi_M = B_M r_i l \beta$$

where B_M is the magnetizing induction required, r_i the inner radius of the magnet ring or segment, l the axial length of the magnet and β (in radians) the angle of the segment or the angle of the magnet ring traversed by the flux.

The same flux goes through the soft iron core in the centre, where the cross-section is smallest

$$\phi_M = B_{Fe}\, bl$$

where B_{Fe} is the induction in the iron and b the distance between the two grooves in which the magnetizing coil is laid. Hence we find that the induction in the centre of the core is

$$B_{Fe} = \frac{B_M r_i \beta}{b};$$

which is apparently higher than B_M (1,2 to 1,4 T). Therefore the core should be made of a soft iron with a very high value of sautration induction, cold rolled sheet silicon iron for instance.

The wall thickness of the stator housing is dimensioned to form the return path of the flux during operation of the motor. Since, however, the inductions required for magnetizing are 4 to 5 times as high as the remanence, this wall thickness will in general be too thin to prevent saturation. An important part of the flux will appear as stray flux and thus cause a high reluctance. A way of improving the return flow of the flux is to slide a tight fitting laminated soft iron ring over the housing. The soft iron poles should extend axially beyond the magnet ring or segment over a distance about equal to the distance between soft core and housing*. It is thus avoided that the stray field occurring at the front end forms an obstruction against thorough magnetization there. Certain types of motors require a special magnetization pattern. This can be realized only by means of a suitably shaped soft iron core and winding arrangement. This particular pattern is usually found empirically, a procedure wherein experience is quickly obtained.

* This is the stator (magnet) thickness plus the air gap.

If such coils are expected to give magnetizing pulses at a rate of more than 10 pulses per minute, they must be cooled. In such cases forced air cooling is usually sufficient. If air channels are to be drilled through the soft iron body it should be only where the flux is weakest. Potting, too, improves natural heat removal.

5.3 Magnetizing Yoke

In some cases it is useful to clamp the part to be magnetized in a magnetizing yoke. Such a yoke can be fitted with small attachments so that it can be used for magnetizing parts of widely different form. Fig. 29, for instance, shows such attachments (pole shoes and pole core) which can be used for magnetizing segments for electric motors. Thus the yoke can be easily adapted to meet a variety of requirements, and it has become a universal instrument in all kinds of laboratories.

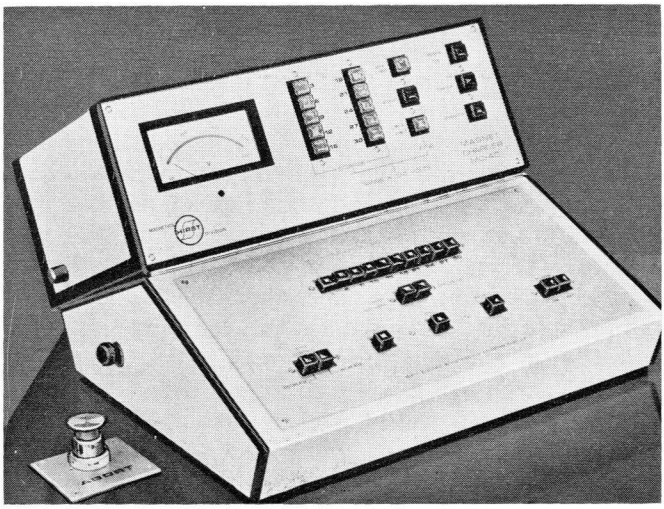

General purpose capacitor discharge magnetizer.
(Courtesy: Hirst Electric Industries Ltd. U.K.)

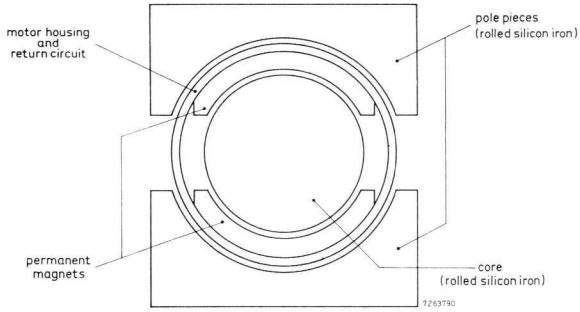

Fig. 29 Special pole shoes and core are applied for magnetizing segments in motors.

To reduce the eddy current losses and the time constant, the magnetizing yoke is preferably made of bonded laminae. Here the air gap has a section of 90×90 mm and can be continuously adjusted to a width of 150 mm. One half of the yoke slides over the other with a large contact area. The contacting parts are precision ground and protected by bellows as is usual in precision engineering. The gap is adjusted by means of a lever via a rack and pinion connection. The magnetizing coils, fed from a capacitor discharge magnetizer, are fitted near the gap to ensure maximum field strength.

In Fig. 30 the maximum attainable field strength between the pole faces is plotted as a function of the pole distance with the initial voltage of the capacitor ($C = 1400$ μF) as parameter. During the magnetizing procedure the pole faces are subjected to great attraction forces. If the clamped object cannot take such great stress, a diamagnetic spacer should be clamped together with the work-piece to reduce the stress. Furthermore a safety switch is provided to ensure that no magnetizing pulse can be sent through the coils if no work-piece is clamped in. Thus it is impossible for the pole pieces to smash into each other. For example the adjustable pole piece can be mechanically connected to a safety switch which is operated only when a work-piece is clamped in. This switch then permits the magnetizing apparatus to operate.

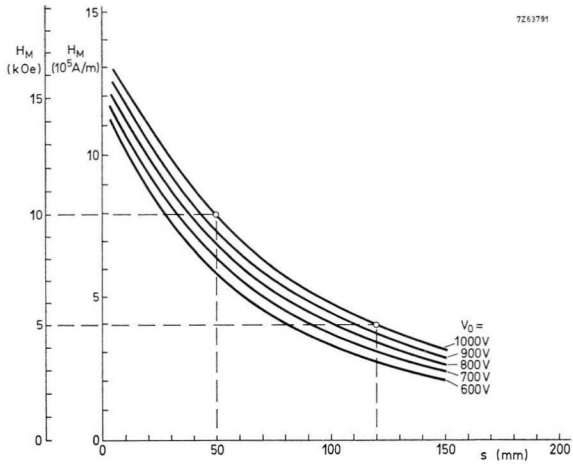

Fig. 30 Maximum field strength between pole faces as a function of the pole separation, with the initial voltage of the capacitor (C = 1400 μF) as a parameter.

This kind of yoke can also be used for magnetizing segments in motors. The segments should be glued or clamped in the housing and the armature should be replaced by a solid core of a high saturation material with low coercivity, such as silicon iron. To facilitate removal of this core after magnetization, an air gap of say 0,5 mm, which must be filled with some non-magnetic material, should be left between core and segments.

The whole assembly is put between the poles of the yoke for magnetizing. Of course the yoke should have pole shoes adapted to receive the circular housing.

A complementary closed magnetic circuit is often not necessary. Two long bars on either side of the air gap may suffice. After the current has been switched off, the system does not remain in the remanent state, but as a load line, the angle of which depends on the length of the bars. When this is some 0,3 to 0,5 metres, the slope of the load line will approximate to that of the practical applications.

5.4 Flux Measurement and Stabilization

To bring the performance of a batch of motors within the required specification it is often necessary to measure the flux in the actual air gap, and successively to reduce this flux to within specified limits. In this way, there is no need to select the magnets used in the motor to a close tolerance, and the effect of manufacturing tolerances in the motor itself can be eliminated. This process is known as stabilization.

The process of stabilization, sometimes called aging or equalization, has been discussed in some detail in section 2.7. The process consists of applying pulses of demagnetizing field to the magnet assembly, and measuring the new working point after each pulse. Each increase in the strength of the demagnetizing pulse causes the magnet load-line to be further displaced, Fig. 31, the final working point being the intersection of the recoil line from the intersection of the last applied load to the assembly load line, Fig. 5.

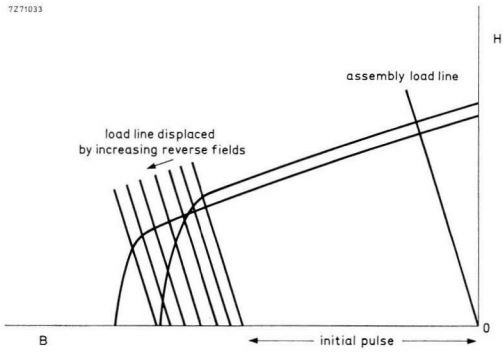

Fig. 31 Increasing reverse fields shifts the load-line further towards the knee of the demagnetization curve.

In order to carry out this operation a reference motor is chosen that has the average required flux in the air gap. The armature is taken out and replaced by a cylindrical core of silicon iron in the centre of which is fixed a Hall probe. The Hall plate should be normal to the lines of force going through the core.

This assembly is inserted between the poles of the magnetizing yoke, the latter not being energized, see Fig. 32. The Hall voltage is now measured, giving a measure of the flux density in the central core and consequently of the flux output of the segments in this particular motor.

To ensure that all motors made from a batch of segments give this same flux output, it is necessary to provide means for magnetizing the motor assembly and then demagnetizing to the level that has been found earlier.

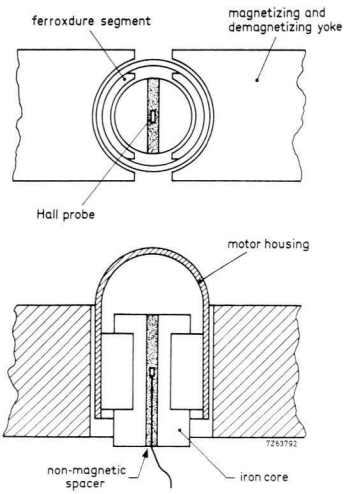

Fig. 32 Location of Hall probe for measurement and field stabilization. The Hall probe may have an offset voltage which should be allowed for.

That means that after magnetizing in the yoke, demagnetizing pulses of increasing magnitude should be given until the Hall probe reading shows that the required flux has been reached. An advantage of this procedure is that the magnets are now stabilized against all stray fields not exceeding the last applied demagnetizing field.

It will be clear that this method of repeated demagnetizing and field measuring can be very time consuming. Therefore equipment has been developed that carries out the whole sequence in a few seconds, see Fig. 33.

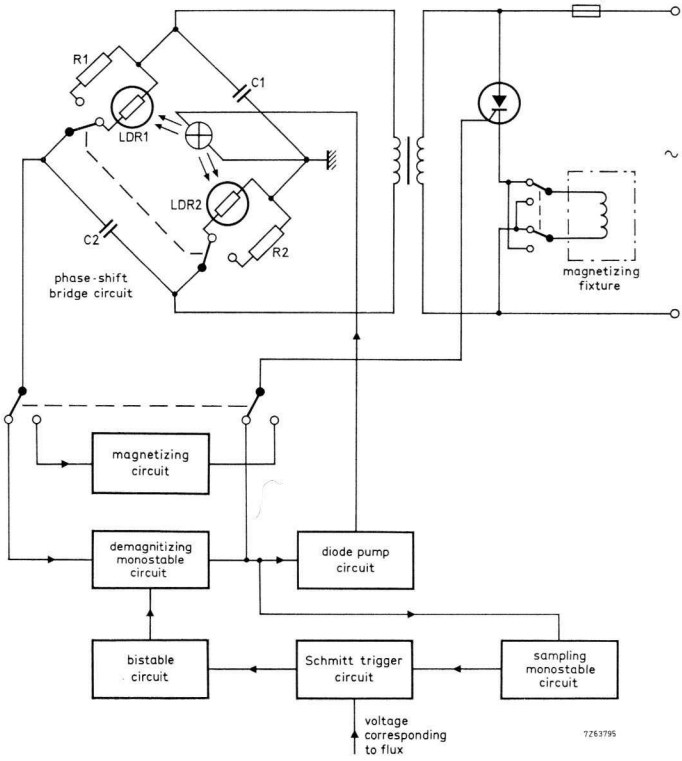

Fig. 33 Set-up for controlled flux reduction ("aging") and stabilization.

Magnetization is achieved by applying a half cycle of the mains to the magnetizing coil via two contactors and a thyristor. The demagnetizing pulses are controlled by the same thyristor, but the contactors are switched so as to reverse the direction of the current. The demagnetizing pulses must start from a low value and gradually increase. This is achieved by slowly increasing the firing angle of the thyristor by a lamp being gradually increased in brightness. This lamp is arranged to illuminate two light dependent resistors, which form opposite branches of a bridge phase-shift network. In this way the phase of the input voltage to the demagnetizing circuit is altered relative to the supply voltage, and the demagnetizing pulses, which are obtained from alternate half cycles of the mains supply, are gradually increasing in magnitude.

The field produced by the segments in the housing assembly is measured by means of a Hall probe situated in the centre core as described before. The measurement is carried out during the half period between two magnetizing pulses. The output voltage from the probe is fed to an amplifier. The output voltage from the amplifier is fed to a meter and to a voltage sampling and measuring circuit. This circuit contains a Schmitt trigger, the output of which is sampled after every demagnetizing pulse for a short time (approx. 2 milliseconds).

When the voltage from the Hall probe has fallen to the required level, an output is obtained from the Schmitt trigger, which is fed to the magnetizing circuit to prevent any further demagnetizing pulses occurring.

A circuit is provided to run the equipment through an automatic sequence, with manually operated magnetize and demagnetize facilities.

Equipment of this kind can easily keep the spread in flux value of a large batch of segments within $\pm 2\%$.

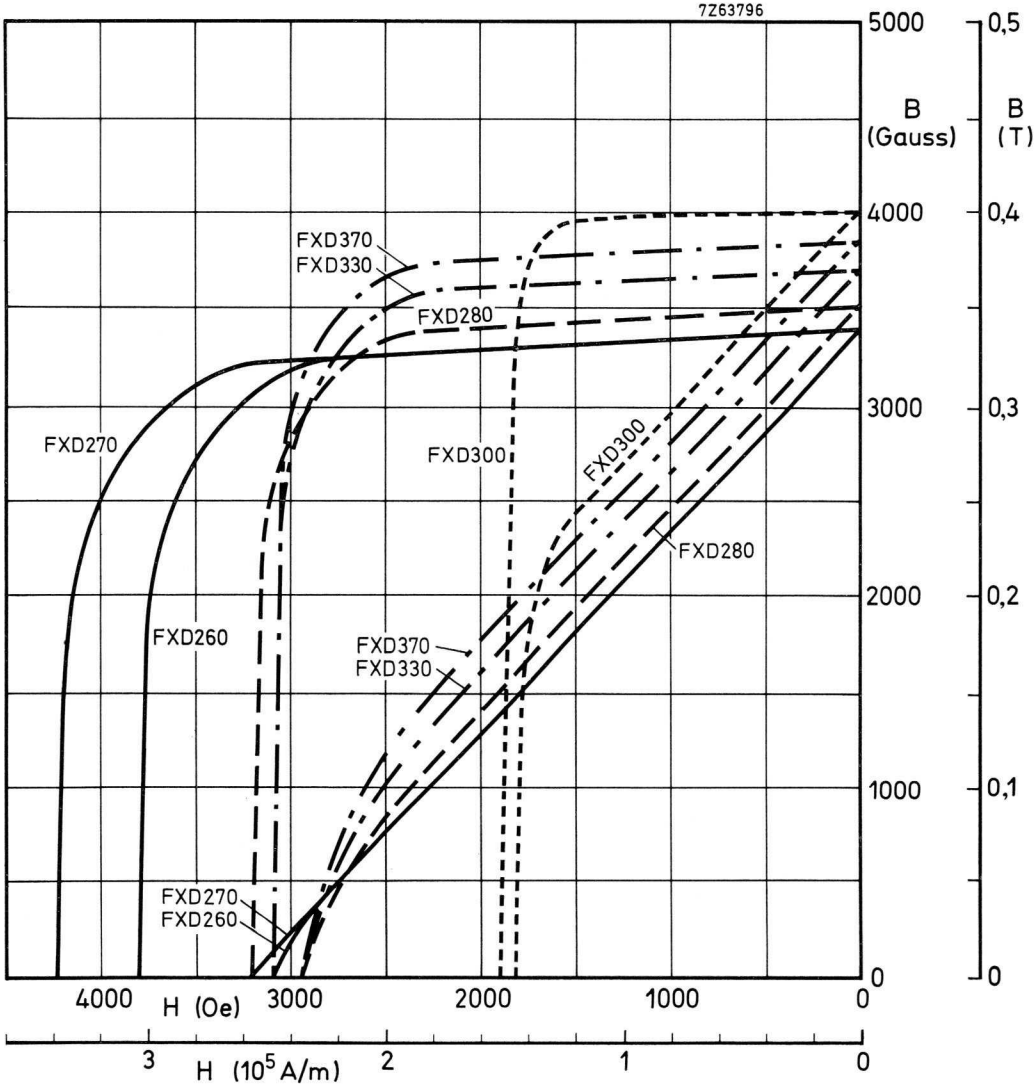

Fig. 34 Demagnetization curves for ferroxdures.

Appendix

Survey of the various grades of ferroxdure that are currently available.

C.G.S. System:

FXD	B_R (gauss)		${}_RBH_c$ (oersted)		${}_RIH_c$ (oersted)		$(BH)_{max}$ (10^6 G.Oe)		specific weight g/cm^3
	min.	typ.	min.	typ.	min.	typ.	min.	typ.	
260	3300	3400	2800	2900	3600	3800	2,4	2,6	4,50
270	3300	3400	2900	3000	4000	4200	2,5	2,7	4,60
280	3400	3500	2800	3000	3000	3200	2,6	2,8	4,60
300	3900	3800	1600	1800	1700	1900	3,4	3,6	4,90
330	3600	3700	2800	3000	2900	3100	3,0	3,2	4,65
370	3800	3850	2750	2950	2900	3100	3,6	3,7	4,75

SI System:

FXD	B_R tesla		${}_RBH_c$ (10^3 A/m)		${}_RIH_c$ (10^3 A/m)		$(BH)_{max}$ (10^3 J/m^3)	
	min.	typ.	min.	typ.	min.	typ.	min.	typ.
260	0,33	0,34	224	232	288	304	19,2	20,8
270	0,33	0,34	232	240	320	336	20,0	21,6
280	0,34	0,35	224	240	240	256	20,8	22,4
300	0,38	0,39	128	144	136	152	27,2	28,8
330	0,36	0,37	224	240	232	248	24,0	25,6
370	0,38	0,385	220	236	232	248	28,8	29,6

Argentina
FAPESA I.y.C.
Av. Crovara 2550
Tel. 652-7438/7478
BUENOS AIRES

Australia
Philips Industries Ltd.
Elcoma Division
67-71 Mars Road
Tel. 42 1261
LANE COVE, 2066, N.S.W.

Austria
Österreichische Philips
Bauelemente Industrie G.m.b.H.
Zieglergasse 6
Tel. 93 26 22
A1072 VIENNA

Belgium
M.B.L.E
80, rue des Deux Gares
Tel. 23 00 00
1070 BRUSSELS

Brazil
IBRAPE S.A.
Av. Paulista 2073-S/Loja
Tel. 278-1111
SAO PAULO, SP.

Canada
Philips Electron Devices
116, Vanderhoof Ave.
Tel. 425-5161
TORONTO 17, Ontario

Chile
Philips Chilena S.A.
Av. Santa Maria 0760
Tel. 39-40 01
SANTIAGO

Colombia
SADAPE S.A.
Calle 19, No. 5-51
Tel. 422-175
BOGOTA D.E. 1

Denmark
Miniwatt A/S
Emdrupvej 115A
Tel. (01) 69 16 22
DK-2400 KØBENHAVN NV

Finland
Oy Philips Ab
Elcoma Division
Kaivokatu 8
Tel. 17271
SF-00100 HELSINKI 10

France
R.T.C.
La Radiotechnique-Compelec
130 Avenue Ledru Rollin
Tel. 357-69-30
PARIS 11

Germany
Valvo G.m.b.H.
Valvo Haus
Burchardstrasse 19
Tel. (0411) 3296-1
2 HAMBURG 1

Greece
Philips S.A. Hellénique
Elcoma Division
52, Av. Syngrou
Tel. 915 311
ATHENS

Hong Kong
Philips Hong Kong Ltd.
Components Dept. (Kowloon Branch)
7th Fl., Wai Yip Industrial Building
41 Tsun Yip St., Kwuntong
Tel. K-42 72 32
HONG KONG

India
INBELEC Div. of
Philips India Ltd.
Band Box House
254-D, Dr. Annie Besant Road
Tel. 457 311 to 15
Prabhadevi, BOMBAY-25-DD

Indonesia
P.T. Philips-Ralin Electronics
Elcoma Division
Djalan Gadjah Mada 18
Tel. 44 163
DJAKARTA

Ireland
Philips Electrical (Ireland) Ltd.
Newstead, Clonskeagh
Tel. 69 33 55
DUBLIN 14

Italy
Philips S.p.A.
Sezione Elcoma
Piazza IV Novembre 3
Tel. 69 94
MILANO

Japan
NIHON PHILIPS
32nd Fl. World Trade Center Bldg.
5, 3-chome, Shiba Hamamatsu-cho
Minato-ku
Tel. (435) 5204-5
TOKYO

Mexico
Electrónica S.A. de C.V.
Varsovia No. 36
Tel. 5-33-11-80.
MEXICO 6, D.F.

Netherlands
Philips Nederland B.V.
Afd. Elonco
Boschdijk 525
Tel. (040) 79 33 33
EINDHOVEN

New Zealand
EDAC Ltd.
70-72 Kingsford Smith Street
Tel. 873 159
WELLINGTON

Norway
Electronica A.S.
Middelthunsgate 27
Tel. 46 39 70
OSLO 3

Peru
CADESA
Jr. Ilo, No. 216
Appartado 10132
Tel. 27 7317
LIMA

Philippines
EDAC
Philips Industrial Dev. Inc.
2246 Pasong Tamo Street
Tel. 88-94-53 (to 56)
MAKATI-RIZAL

Portugal
Philips Portuguesa S.A.R.L.
Av. Eng. Duharte Pacheco 6
Tel. 68 31 21
LISBOA 1

South Africa
EDAC (Pty.) Ltd.
South Park Lane
New Doornfontein
Tel. 24/6701-2
JOHANNESBURG

Spain
COPRESA S.A.
Balmes 22
Tel. 329 63 12
BARCELONA 7

Sweden
ELCOMA A.B.
Lidingövägen 50
Tel. 08/67 97 80
10250 STOCKHOLM 27

Switzerland
Philips A.G.
Edenstrasse 20
Tel. 01/44 22 11
CH-8027 ZUERICH

Taiwan
Philips Taiwan Ltd.
San Min Building, 3rd Fl.
57-1, Chung Shan N. Road
Section 2
P.O. Box 22978
Tel. 553101-5
TAIPEI

Turkey
Türk Philips Ticaret A.S.
EMET Department
Gümüssuyu Cad. 78-80
Tel. 45.32.50
Beyoglü, ISTANBUL

United Kingdom
Mullard Ltd.
Mullard House
Torrington Place
Tel. 01-580 6633
LONDON WC1E 7HD

United States
North American Philips
Electronic Component Corp.
230, Duffy Avenue
Tel. (516) 931-6200
HICKSVILLE, N.Y. 11802

Uruguay
Luzilectron S.A.
Rondeau 1567, piso 5
Tel. 9 43 21
MONTEVIDEO

Venezuela
C.A. Philips Venezolana
Elcoma Department
Av. Principal de los Ruices
Edif. Centro Colgate
Apartado 1167
Tel. 36.05.11
CARACAS

Printed in The Netherlands

32 321 323 8-74 9399 266 02201